

1 **Structural, lithological and geodynamic controls on geothermal activity in the**
2 **Menderes geothermal Province (Western Anatolia, Turkey)**

3
4 Vincent ROCHE^{a*}, Vincent BOUCHOT^a, Laurent BECCALETTO^a, Laurent JOLIVET^b,
5 Laurent GUILLOU-FROTTIER^a, Johann TUDURI^a, Erdin BOZKURT^{c,d}, Kerem OGUZ^e and
6 Bulent TOKAY^d

7
8 *^aISTO, UMR7327, Université d'Orléans, CNRS, BRGM, F-45071 Orléans, France*

9 *^bSorbonne Université, CNRS-INSU, Institut des Sciences de la Terre Paris, ISTeP UMR 7193, F-75005*
10 *Paris, France*

11 *^cMiddle East Technical University, Department of Geological Engineering, Üniversiteler Mahallesi,*
12 *Dumlupınar Bulvarı No: 1, 06800 Ankara, Turkey*

13 *^dCenter for Global Tectonics & State Key Laboratory of Geological Processes and Mineral Resources,*
14 *China University of Geosciences, Wuhan, 388 Lumo Road, Hongshan District, Wuhan 430074, Hubei*
15 *Province, China*

16 *^eMunicipality of Salihli, Manisa, Turkey*

17
18 *Corresponding author: V. Roche, ISTO, 1A rue de la Férollerie, 45071, Orléans, France

19 (e-mail: vincent.roche@cnrs-orleans.fr; Tel : +33 6 32 52 98 18)

20
21 **Abstract:**

22 Western Turkey belongs to the regions with the highest geothermal potential in the world,
23 resulting in significant electricity production from geothermal resources located predominantly in
24 the Menderes Massif. Although geothermal exploitation is increasingly ongoing, geological and
25 physical processes leading to the emplacement of geothermal reservoirs are hitherto poorly
26 understood. Several studies on the Menderes Massif led to different interpretations of structural
27 controls on the location of hot springs and of the heat source origin. This paper describes

28 geological evidence showing how heat is transmitted from the abnormally hot mantle to the
29 geothermal reservoirs. On the basis of field studies, we suggest that crustal-scale low-angle
30 normal faults convey hot fluids to the surface and represent the first-order control on geothermal
31 systems. At the basin-scale, connected on low-angle normal faults, kilometric high-angle transfer
32 faults are characterized by dilational jogs, where fluids may be strongly focused. In addition,
33 favourable lithologies in the basement (*e.g.* karstic marble) could play a critical role in the
34 localization of geothermal reservoirs. Finally, a compilation of geochemical data at the scale of
35 the Menderes Massif suggests an important role of the large mantle thermal anomaly, which is
36 related to the Hellenic subduction. Heat from shallow asthenospheric mantle is suggested to be
37 conveyed toward the surface by fluid circulation through the low-angle faults. Hence, geothermal
38 activity in the Menderes Massif is not of magmatic origin but rather associated with active
39 extensional tectonics related to the Aegean slab dynamics (*i.e.* slab retreat and tearing).

40

41 **Keywords:** Menderes Massif, structural control, detachment, transfer fault, hot mantle anomaly,
42 slab dynamics

43

44 **1. Introduction:**

45 The high heat flow driving active geothermal systems is often believed to find its source in
46 portions of crust invaded by magmas, but some of significant geothermal provinces are considered
47 amagmatic namely not of magmatic origin in terms of heat source (*i.e.* no magmatic intrusions in
48 the upper crust). In this case, large-scale processes (*e.g.* slab dynamics) inducing large-scale
49 thermal anomalies are favoured, as for the Basin & Range Province in the Western US. In this
50 extensional context, geothermal systems have been described as amagmatic in origin (*e.g.* Benoit
51 1999; Blackwell *et al.* 2000; Faulds *et al.* 2004; 2011). The exact origin of heat remains debated
52 and, for instance, magmatic underplating under the overriding plate (Wannamaker *et al.* 2006)

53 and/or shear heating in the mantle in actively deforming area (*e.g.* Roche *et al.* 2018) are some
54 hypothesis of heat source possibilities. Despite the well-documented existence of large-scale
55 seismic velocity anomalies in the mantle of the Eastern Mediterranean region (*e.g.* De Boorder *et*
56 *al.* 1998), very few studies have actually considered such amagmatic geothermal provinces in
57 their large-scale geodynamic contexts (*e.g.* Roche *et al.* 2015; 2016; 2018; Gessner *et al.* 2017).
58 The path of heat transport from mantle to surface, either conductive or through advection of hot
59 fluids, remains to be described in such environments. The Menderes Massif is one of the best
60 examples where such a description can be done, from the mantle to the actively extending crust,
61 up to the geothermal reservoirs.

62 The Menderes Massif is recognized as an active geothermal area where extensional or
63 transtensional tectonics is accompanied by elevated heat flow values ($\sim 100 \text{ mW m}^{-2}$), which
64 appear to extend to almost the entire Aegean domain (Erkan 2014; 2015). There, high heat flow
65 estimated by Jongsma (1974) may correspond to the low *P*- wave seismic velocity zone described
66 by Piromallo and Morelli (2003). Surprisingly, magmatic activity and related volcanism have been
67 very sparse there in the recent period (*i.e.* Pliocene and Quaternary); the unique volcanic activity
68 occurred in the Kula volcanic field during the Quaternary between 2 and 0.2 Ma (*e.g.* Richardson-
69 Bunbury 1996; Bunbury *et al.* 2001; Maddy *et al.* 2017) where geothermal activity is absent.
70 Existing models suggest probable magmatic reservoirs in the upper crust as heat source of the
71 geothermal system in this area, more or less connected with the Kula basaltic activity (*e.g.* Simsek,
72 1985; Filiz *et al.* 2000; Karamanderesi and Helvacı 2003; Yilmazer *et al.* 2010; Bülbül *et al.* 2011;
73 Özen *et al.* 2012; Özgür *et al.* 2015; Ozdemir *et al.* 2017; Alçıçek *et al.* 2018). Nonetheless, others
74 authors have also suggested a deeper and larger heat source triggered by slab dynamics (*i.e.*
75 asthenospheric mantle flow due to slab rollback and tearing; *e.g.* Kaya 2015; Roche *et al.* 2015;
76 2016; 2018; Gessner *et al.* 2017). It is then worth studying the consequences of these processes
77 on the distribution of heat at the surface. In this case, recent tectonic activity and related graben

78 structures have a major interest because they could control the fluid flow processes (*e.g.* Tarcan
79 and Gemici 2003; Faulds *et al.* 2010; Haizlip *et al.* 2013; Kocyigit 2015; Kaya 2015; Haklidir *et*
80 *al.* 2015).

81 Consequently, this study is dedicated to a multi-scale analysis of the different identified
82 features of several geothermal fields of the Menderes Massif. We present a detailed structural
83 analysis of main geothermal fields (*i.e.* Salihli, Alaşehir, Salavatlı and Seferihisar, Kızıldere,
84 Germencik) to better characterize the fluid flow pattern. It is critical to evaluate which type of
85 faults and which parts of them are most favourable for focusing geothermal activity. Our results
86 are then discussed at different scales including that of the “Menderes geothermal Province”. At
87 the scale of lithosphere-mantle interactions, we use a broad compilation of mantle-He and oxygen-
88 hydrogen isotopic data to propose and discuss a new conceptual model explaining the regional
89 thermal anomaly with reference to geodynamic processes.

90

91 **2. Geological setting**

92 2.1. The Eastern Mediterranean region

93 During the Cenozoic, the Eastern Mediterranean region (Fig. 1a) has undergone a two-step
94 tectono-metamorphic evolution. Firstly, in the late Cretaceous-Eocene, the convergence of Africa
95 and Eurasia has led to the closure of the Izmir-Ankara Ocean and to the accretion of subducting
96 continental and oceanic lithospheres (Bonneau and Kienast 1982; Dercourt *et al.* 1986; Jolivet
97 and Brun 2010). Secondly, since the Oligo-Miocene, the kinematics in Mediterranean region has
98 been mainly controlled by the southward retreat of the African slab responsible for back-arc
99 extension (*e.g.* Malinverno and Ryan 1986; Jolivet and Faccenna 2000; Jolivet and Brun 2010;
100 Ring *et al.* 2010). The Oligo-Miocene geological evolution of the Aegean region, including the
101 Menderes Massif and the Cyclades, results from this episode of slab roll-back (*e.g.* Seyitoglu and

102 Scott 1991; Seyitoğlu *et al.* 1992; Seyitoglu and Scott 1996; Jolivet *et al.* 1996). In addition, recent
103 studies based on geochemical analyses (*e.g.* Dilek and Altunkaynak 2009; Ersoy *et al.* 2010;
104 Prelevic *et al.* 2012), on tomographic models (*e.g.* De Booder *et al.* 1998; Biryol *et al.* 2011;
105 Salaün *et al.* 2012) and on tectonic and magmatic evolution in this area (Dilek and Altunkaynak
106 2009; Jolivet *et al.* 2015; Menant *et al.* 2016; Govers and Fichtner 2016) invoke the particular
107 slab dynamics beneath western Turkey, which would be characterized by a slab tear since the
108 Miocene (Jolivet *et al.* 2015) (Fig. 1a). The complex geometry of subduction zones and the tight
109 arcs characterizing the Mediterranean region as a whole are direct consequences of slab retreat
110 and slab tearing (Wortel and Spakman 2000; Spakman and Wortel 2004; Faccenna *et al.* 2004;
111 Govers and Wortel 2005; Faccenna *et al.* 2006). Beside the heat wave caused by the advection of
112 hot asthenosphere to shallow depths during retreat, slab tearing tends to efficiently localize
113 deformation, and to facilitate high-temperature metamorphism, crustal melting, granitic intrusions
114 and fluid circulations (Jolivet *et al.* 2015; Menant *et al.* 2016; Roche *et al.* 2018). Therefore,
115 magmatic activity during the Miocene was intense in western Turkey, but it has significantly
116 decreased since 12 Ma (*e.g.* Ersoy *et al.* 2010). In addition, this slab dynamics has a direct
117 consequence on Moho depth, estimated only at ~ 25 – 30 km in the Menderes Massif (based on
118 geophysical data such as receiver functions computed from teleseismic earthquakes from
119 Karabulut *et al.* (2013); deep seismic reflection data from Cifci *et al.* (2011); Bouguer gravity data
120 from Altinoğlu *et al.* 2015 and conductivity data from Bayrak *et al.* (2011)).

121 The current tectonic evolution in this region is mainly controlled by the westward motion
122 of Anatolia (Reilinger *et al.* 2006) and by N-S extension, both consequences of the same slab roll-
123 back process complicated by several episodes of slab tearing (*e.g.* Faccenna *et al.* 2006; Jolivet *et*
124 *al.* 2013; 2015). This direction of extension is also well constrained by the orientation of regional-
125 scale anisotropic fabrics, suggesting a large-scale viscous flow in the lower crust and lithospheric
126 mantle since the Miocene (Endrun *et al.* 2011).

127

128 2.2. The Menderes Massif

129 The Menderes Massif is located in the back-arc domain of the Hellenic subduction zone in
130 the western part of Turkey (Figs. 1a and 1b), and constitutes a part of the Anatolide-Tauride block.
131 After a first episode of nappe stacking and crustal thickening (*e.g.* Collins and Robertson 1998;
132 Ring *et al.* 1999; Gessner *et al.* 2001a), the thickened crust of the Menderes Massif has undergone
133 a NNE-SSW post-orogenic extension stage since the Oligo-Miocene (*e.g.* Seyitoglu and Scott
134 1991; Seyitoglu *et al.* 1992; Bozkurt and Oberhänsli 2001; Bozkurt *et al.* 2011). Considered as a
135 single large metamorphic core complex, this massif has recorded a controversial two-stage
136 exhumation process. According to Ring *et al.* (2003), these two stages are symmetrical, first along
137 the south-dipping Lycian and north-dipping Simav detachments on the southern and northern
138 edges of the massif, and then located in the Central Menderes Massif (CMM) along the Alaşehir
139 and the Büyük Menderes detachments (Fig. 1b). But Seyitoglu *et al.* (2004) challenged the first
140 stage of exhumation suggesting that this massif was exhumed initially as an asymmetric core
141 complex in the Early Miocene. In any case, this post-orogenic extension has led to the exhumation
142 of three submassifs, from north to south: the Gördes, Ödemiş (corresponding to the CMM) and
143 Çine submassifs. These submassifs are separated by E-W striking half-grabens that are seismically
144 active. The northern part of the Gördes submassif is limited in the north by the Simav graben, the
145 Ödemiş submassif by the Alaşehir graben (also known as Gediz graben) to the north, and by the
146 Büyük Menderes graben to the south (Fig. 1b, see more details in the Appendix for the studied
147 grabens).

148 Post-orogenic extension was thus accommodated by three main detachment faults (*i.e.* low-
149 angle normal faults) in the central and northern submassifs, namely:

- 150 (i) the Büyük Menderes detachment along the northern margin of the Büyük Menderes
151 graben with top-to-the-S kinematic criteria (Fig. 1b; *e.g.* Emre and Sözbilir, 1997;
152 Gessner *et al.* 2001b; Ring *et al.* 2003);
- 153 (ii) the Alaşehir detachment (also named Gediz detachment, Lips *et al.* 2001) along the
154 southern margin of the Alaşehir graben with top-to-the-N sense of shear (Fig. 1b;
155 *e.g.* Emre, 1992; Hetzel *et al.* 1995a; 1995b; Gessner *et al.* 2001b; Sözbilir 2001;
156 Seyitoglu *et al.* 2002; Işık *et al.* 2003; Bozkurt and Sözbilir 2004; Hetzel *et al.* 2013)
157 and
- 158 (iii) the Simav detachment, later cut by the high angle Simav normal fault that bounds to
159 the south the Simav graben with top-to-the-NE kinematic indicators (Fig. 1b; *e.g.*
160 Seyitoglu 1997; Isik *et al.* 1997; Isik and Tekeli, 2001; Işık *et al.* 2004).

161 However, the exhumation history of the Menderes Core complex and the multi-staged
162 activity of the detachments remain matters of debate. Several authors suggest that the Alaşehir
163 graben formation is controlled by (i) low-angle normal faults that have been active since the
164 inception of the basin, and then by (ii) more recent high-angle faults crosscutting the earlier-ones
165 (*e.g.* Hetzel *et al.* 1995a; 1995b; Emre and Sozbilir 1997; Sozbilir 2001; Oner and Dilek 2011).
166 For others, the initiation of the graben involved high-angle normal faults that gradually became
167 low angle with time (*e.g.* Gessner *et al.* 2001b; Bozkurt 2001; Seyitoğlu *et al.* 2002; Purvis and
168 Robertson 2005; Ciftci and Bozkurt 2009; 2010; Demircioğlu *et al.* 2010; Seyitoğlu *et al.* 2014).
169 According to Seyitoğlu and Işık (2015), this last hypothesis may explain the large range values of
170 ages from the Alaşehir detachment, explaining a continuum of deformation since Early Miocene
171 in the framework of a rolling hinge model (Buck 1988) for the formation of the grabens and
172 exhumation of the CMM (*e.g.* Gessner *et al.* 2001b; Seyitoglu *et al.* 2002; 2014). Note that syn-
173 extensional Miocene granitoid intrusions are also recorded in the footwall of the Alaşehir and
174 Simav detachments (*e.g.* Hetzel *et al.* 1995b; Isik *et al.* 2003; 2004).

175 The early Miocene evolution of the Menderes Massif is dominated by high-angle E-W
176 striking normal faults that root into (Seyitoglu *et al.* 2002) or cut the current low-angle normal
177 faults (*e.g.* Koçyigit *et al.* 1999; Yılmaz *et al.* 2000), and control basin sedimentation (*i.e.* the
178 initiation of the Alaşehir and Büyük Menderes grabens formation; *e.g.* Seyitoglu 1997; Seyitoglu
179 *et al.* 2002). During Pliocene-Quaternary times, another set of high-angle normal faults is
180 recorded, controlling the youngest grabens such as the Küçük Menderes and Simav grabens
181 (Seyitoglu *et al.* 2004) and the current geometry of the basin (Bozkurt and Sozbilir 2004; Kent *et*
182 *al.* 2016). Furthermore, an additional distributed strike-slip tectonics with a normal component is
183 well observed in the Alaşehir graben with high-angle N-S striking faults crosscutting the Neogene
184 sediments (*e.g.* Çiftçi and Bozkurt 2010; Yilmazer *et al.* 2010; Ozen and Dilek 2011) and affecting
185 the basement of the Menderes Massif (see black dotted line in the Alaşehir graben in Fig. 1b).
186 Similar strike-slip faults are observed in the Büyük Menderes graben, which can be interpreted as
187 transfer faults (*e.g.* Çifçi *et al.* 2011).

188

189 **3. Geothermal setting in the Menderes Massif**

190 3.1. Thermal anomalies at different scales

191 At first glance, there is a strong correlation between the distribution of geothermal fields
192 with its hot springs and the location of detachments (Fig. 1b). According to recent studies (*e.g.*
193 Roche *et al.* 2015; 2016; 2018; Kaya, 2015; Gessner *et al.* 2017), these large-scale structures may
194 represent the first-order control on geothermal fields in this massif. In that instance, Gessner *et al.*
195 (2017) showed that most of hotter thermal springs are located in areas of structural complexity
196 such as Seferihisar, Denizli, Salihli and Alaşehir. Similar correlations between high heat flow
197 values and complex graben structures are emphasized by many studies (Tezcan 1995; Pfister *et*
198 *al.* 1998; Erkan 2014; 2015). For instance, Erkan (2014) estimated heat flow values of 85 – 90
199 mW m⁻², locally higher than 100 mW m⁻² in the northeastern part of the Alaşehir graben. These

200 data are in accordance with locations of several geothermal reservoirs of interest, but also with
201 shallow Curie-point depth (CPD) published in the Menderes Massif area (Aydin *et al.* 2005;
202 Dolmaz *et al.* 2005; Bilim *et al.* 2016). According to Bilim *et al.* (2016), the average of CPD in
203 the whole Menderes area (assumed to represent the depth of the 580 °C isotherm, Schlinger 1985;
204 Ross *et al.* 2006) is *ca.* 9.5 km with a shallowest point at 6.21 km around the Kula basaltic area.
205 A thermal anomaly thus encompasses the whole Menderes Massif. The same authors also suggest
206 that locations of geothermal fields belonging to the Büyük Menderes graben area coincide with
207 the lowest values of the magnetic intensity, which are aligned along the boundary fault of this
208 graben. Furthermore, using the magnetotelluric method through the northern part of the Menderes
209 Massif, Ulugergerli *et al.* (2007) proposed a large partial melting zone located at ~ 12 km depth
210 and deep intrusions (*i.e.* ~ 15 km depth) located below the Simav graben and the Kula volcano,
211 therefore suggesting abnormal high temperature values.

212 To sum up, all these studies confirm that thermal anomalies in the Menderes Massif are
213 observed with different wavelengths (*i.e.* crustal-scale to geothermal field-scale), thus different
214 depths. The short wavelength anomalies result from shallow depth processes and those with long
215 wavelength (crustal-scale) from deep processes, and thus large-scale dynamics (*e.g.* Roche *et al.*
216 2015; 2016; 2018; Gessner *et al.* 2017). However, the plumbing system (*i.e.* circulation pathways)
217 of such hot crustal fluids are not yet properly understood.

218

219 3.2. Synthesis of fluids and isotopes

220 3.2.1. Studies on oxygen and hydrogen isotopes of the main geothermal fluids

221 Many studies on the isotopic composition of water samples in the CMM area have been
222 performed (Fig. 2; Filiz *et al.* 2000; Özgür 2002; Tarcan and Gemici 2003; Özen *et al.* 2012; Baba
223 *et al.* 2014). To the first order, they show that most of the data from the Alaşehir and the Büyük
224 Menderes grabens are close to the global meteoric water line (GMWL) thus indicating a meteoric

225 origin for most of the geothermal fluids (Figs. 2b and 2c). Indeed, the distribution of isotopic
226 compositions of the thermal waters in Salihli, Aydın-Germencik, Salavatlı and Denizli-Kızıldere
227 geothermal fields shows a meteoric origin. However, some variations in isotopic distributions can
228 be noted. There is a clear $\delta^{18}\text{O}$ shift from the MMWL (Mediterranean Meteoric Water Line) and
229 cold-water values (empty symbols in Fig. 2b) that indicate strong water-rock interaction for all
230 geothermal fields (Figs. 2b and 2c). For example, the isotopic distribution of hot waters in
231 Kurşunlu and in greenhouses well is located below the GMWL, which suggests a probable mixing
232 of deep and shallow thermal waters (Özen *et al.* 2012). Bülbül *et al.* (2011) reported a similar
233 observation from the Alaşehir geothermal field, suggesting that thermal water reservoirs are fed
234 by ground waters of dominant meteoric origin. They estimated cold-water contributions to thermal
235 waters ranging from 75 to 95%. Moreover, the Seferihisar geothermal field, in the Cumaovası
236 basin, shows additional variations in isotopic compositions (Fig. 2d): isotopic values approach the
237 isotopic value of Aegean sea water, implying a mixing with seawater related to the proximity of
238 the Mediterranean Sea (Tarcan and Gemici 2003). Similar signatures are observed in the Söke
239 geothermal field (Simsek 2003), with slight deviations from the MMWL line of isotopic
240 distribution, implying an evaporation effect on cold-waters (Fig. 2d). The isotopic composition of
241 thermal waters indicates that they are of meteoric origin and then mixed with seawater in the
242 western part of Söke, particularly near the coast.

243

244 3.2.2. Helium isotopic signature

245 In a tectonically active continental setting, the presence or the absence of mantle helium
246 (^3He) in hydrothermal fluids can constrain the relationships between tectonics, magmatism and
247 fluid circulation in faulted settings (O'Nions and Oxburgh 1988; Marty *et al.* 1992; Kennedy *et al.*
248 *et al.* 1997; Kulongoski *et al.* 2005; Pik and Marty 2009). It has been established that the $^3\text{He}/^4\text{He}$
249 ratio can be used as tracer of the competing influence of crustal vs. mantle volatiles in various

250 tectonic settings (Mutlu *et al.* 2008). Based on the analyses of water and gas samples, and/or fluid
251 inclusion trapped in calcite, many studies have discussed the isotopic composition of He in the
252 Eastern Mediterranean region (Güleç 1988; Güleç *et al.* 2002; Shimizu *et al.* 2005; Güleç and
253 Hilton 2006; Mutlu *et al.* 2008; Pik and Marty 2009; Karakus 2015). Below, we present a new
254 compilation of recent isotopic studies using the classification of Pik and Marty (2009) (Fig. 3).

255 In the Aegean domain, the Corinth rift shows a crustal signature while the Hellenic volcanic
256 arc is characterized by high values of $^3\text{He}/^4\text{He}$ ratio, Ra ($> 15\%$ of mantle-He) suggesting a mantle
257 origin (Fig. 3a). In addition, estimated $^3\text{He}/^4\text{He}$ ratios of samples normalized to the atmospheric
258 $^3\text{He}/^4\text{He}$ ratio range from 0.10 to 1.44 in the western part of Anatolia (Figs. 3a and 3b). These
259 values are significantly higher than the crustal production value of 0.05 (Mutlu *et al.* 2008).
260 Karakuş (2015) added new data on the $^3\text{He}/^4\text{He}$ ratios for the Simav geothermal field (values range
261 from 1.36 to 1.57). The highest values of helium ratio correspond to the Quaternary alkaline
262 activity of Kula volcano and to the Pliocene Denizli volcanics (2.52) along the Alaşehir and the
263 eastern segment of the Büyük Menderes grabens (Fig. 3b). These results reveal a mixed origin for
264 helium between mantle and continental crust components.

265

266 **4. Analysis of the tectonic and structural settings of geothermal fields in the Menderes** 267 **Massif at local and regional scale**

268

269 In this chapter, we summarize the structural framework of several geothermal fields, in order
270 to identify the main conduits for geothermal fluid flow and related reservoirs. Our field survey
271 consisted of (i) field mapping in order to complement the existing geological and geothermal maps
272 and (ii) structural data acquisition and (iii) general cross-sections. We have first focus on the
273 Alaşehir graben (Fig. 1b), where numerous geothermal wells have been drilled by MTA (General
274 Directorate of Mineral Research and Exploration of Turkey) or by private companies since the
275 1980s, and where two most important geothermal fields are recognized (Salihli and Alaşehir, Fig.

276 4a). We will then focus on the Germencik and Salavatlı geothermal fields located along the
277 northern margin of the Büyük Menderes half-graben (Fig. 1b). Finally, the structural framework
278 of the Seferihisar geothermal field is also provided (Fig. 1b). A brief description of all these
279 geothermal systems is presented in the Appendix. They are generally characterized by medium-
280 to high-enthalpy, with reservoir temperature values ranging from 120 to 287 °C (*e.g.*
281 Karamanderesi, 2013; Baba *et al.* 2015).

282

283 4.1. Structural features of the Salihli geothermal field

284 At regional-scale, the Alaşehir detachment is one of the best-preserved crustal structure in
285 the study area (Fig. 5a). Both metamorphic rocks and Miocene intrusions in the footwall of the
286 detachment present a pervasive network of kilometric to millimetric structures developed from
287 the ductile-brittle transition to the brittle deformation field during extension and exhumation (Fig.
288 4b) (*e.g.* Emre 1992; Hetzel *et al.* 1995a; 1995b; Isik *et al.* 2003). Close to the main contact
289 between the Menderes basement rocks and Neogene sediments, the foliation of basement rocks
290 strikes E-W with low to moderate dip values toward the north and carries a N-S trending stretching
291 lineation (Fig. 4). Most ductile kinematic indicators are top-to-the-NNE. All lithologies are
292 deformed by asymmetric structures and folds at various scales consistent with top-to-the-NNE
293 shear sense such as asymmetric boudinaged quartz veins within tight overturned folds indicating
294 a top-to-the-NE sense of shear (Fig. 5b). On the other hand, ductile-brittle fault system
295 corresponds to listric and gently dipping centimetric to decametric faults within schist and marble
296 layers that may reactivate and (or) cross-cut low-angle ductile shear zones (Fig. 5c). This brittle
297 stage is associated with slickenlines and kinematic indicators indicating also top-to-the-NNE
298 motion (Fig. 4a, #2). Finally, the brittle detachment fault plane is well observed in the landscape
299 (Fig. 5a), controlling the present-day topography of the CMM at regional scale and strikes E-W
300 with a moderate dip toward the north (Fig. 4a, #8). It is associated with a thick (approximately 50

301 cm to 3 m) zone of cataclasites or a thick quartz-breccia vein (Fig. 5d), which locally hosts Sb-
302 Hg(-Au) ore deposits (Larson and Erlor 1993). Fault plane and associated striae (*e.g.* Fig. 4a, #3
303 and #4) are consistent with a NNE-SSW extension. In addition, vein networks mostly filled by
304 calcite or quartz in the footwall of the detachment (Fig. 5e) present an approximately NW-SE (*i.e.*
305 parallel to the detachment) and NE-SW preferred orientations (*i.e.* perpendicular to the
306 detachment) (Fig. 4a, #2). This shows evidence of a significant older fluid circulation in the fault
307 plane during the exhumation of the deeper parts of the Menderes Massif.

308 In the entire studied area, faults that are particularly abundant play a major role in the
309 formation and development of longitudinal and transverse valleys (*e.g.*, Kurşunlu valley, Alaşehir
310 graben). Three types of plurimetric to kilometric faults, particularly frequent in this area, are
311 observed in the field (Fig. 4a). The first one is characterized by NNE-dipping normal faults (*i.e.*
312 E-W trending) and the second one is defined by sub-vertical N-S striking strike-slip faults (Figs.
313 4a, #2; 6a and 6b). In the second case, slickenlines are gently plunging consistently 15 to 30°N
314 (Figs. 6a and 6c) and kinematic indicators indicate a main dextral movement with a slight normal
315 component. Locally, these faults are accompanied with a cluster of calcite veins as dilational jog
316 structures (Fig. 6d). The third type of faults consists in a set of conjugate faults strikes NE-SW
317 and dips with an approximately 60° mean dip angle, is well developed in quartzite levels in the
318 Kurşunlu valley (Fig. 4a, #2). The different fault sets, including the detachment and the associated
319 high-angle E-W conjugate normal faults and the N-S strike-slip faults to NE-SW faults, are
320 compatible with N-S extension, where strike-slip faults act as transfer zones between extensional
321 blocks. All these faults affect the basement and the Neogene sediments, but the chronologic
322 relationships are not clear in the field.

323

324 4.2. Structural features of the Alaşehir geothermal field

325 The Alaşehir geothermal field is located between Alaşehir and Salihli in the eastern part of
326 Alaşehir graben. It is one of the most important geothermal areas characterized by the highest
327 reservoir temperature (287 °C) ever reached in Turkey (in a deep well, 2750 m, from Baba *et al.*
328 (2015), Table 1). As for the Salihli geothermal field, the recent tectonic activity is assumed to
329 control the location of the thermal springs and related geothermal reservoirs (Bülbül *et al.* 2011).
330 In this area, the detachment fault plane is attested by the development of a thick zone (~ 1 m) of
331 cataclasites (Fig. 7a). It consists of yellow and red foliated cataclasites directly overlain by
332 unaltered Neogene sediments (Fig. 7b). Close to the kinematics recorded in the area of Salihli,
333 striae are compatible with a NE-SW extension (Fig. 7a and 4, #7). Additional low-angle normal
334 faults in the hanging-wall of the detachment are observed between 1 metre-thick cataclasites and
335 sediments (Figs. 7c, 7d and 7e). Locally pseudotachylytes are observed (Fig. 7f) and medium-
336 angle normal faults in sediments merge with the main fault plane (Fig. 7g). According to Hetzel
337 *et al.* (2013), this brittle deformation stage observed in the Alaşehir detachment system was active
338 from ~ 9 Ma to 4 – 3 Ma. This may be consistent with rapid Pliocene cooling inferred from
339 published thermochronological data (Gessner *et al.* 2001b; Ring *et al.* 2003). While the Alaşehir
340 detachment is well defined in the landscape at Salihli, it is however often crosscut by a set of E-
341 W high-angle north-dipping normal faults in the Alaşehir area (Figs. 4b and 8a). Brittle structures,
342 shallow- and steeply-dipping faults present a marked consistency of the extension direction (Fig.
343 4a, #6). Locally, fluid circulation occurs along fault planes (Fig. 8b), suggesting that these faults
344 may also control meteoric fluid circulations. The absence of any hot springs close to the E-W
345 striking faults suggest that these faults play as recharge pathway for reservoirs at depth.

346 Furthermore, another set of faults is observed at some places. At landscape-scale, in the
347 south-east of Alaşehir, we identified triangular facets within synrift sediments due to NW-SE
348 trending high-angle normal fault (Fig. 8c). The latter are horizontally offset from 2 km toward the

349 south in the Narlıdere area, defining a NE-SW transfer fault (Figs. 8c and 1b for the location).
350 Similar features are also observed in the Dereköy traverse valley, close to the Horzum Turtleback
351 structure described by Seyitoglu *et al.* (2014). There, we identified a N-S striking high-angle fault
352 (Fig. 8d). Fault kinematics indicates an early sinistral movement followed by normal movement
353 (Figs. 4a, #5 and 8d). The synrift sediments are offset southward and face the Paleozoic basement
354 of the detachment footwall across the valley, indicating the presence of left-lateral strike-slip fault
355 in the vicinity of the Horzumsazdere geothermal system (black line in Fig. 4a). Close to the
356 detachment and to these N-S strike-slip faults, a weak fumarole activity associated with a probable
357 acidic alteration (with the typical H₂S smell) affects Neogene sediment deposits (Fig. 8e). Down
358 in the valley, several thermal springs (medium temperatures ranging around 25 and 30 °C) reach
359 the surface in Neogene sediments where they form travertines.

360

361 4.3. Structural features of the Salavatlı and Germencik geothermal fields

362 South of the CMM, the Salavatlı and Germencik geothermal fields (Table 1 for more
363 information) are respectively located on the northern flank of the Büyük Menderes graben
364 between Sultanhisar and Köşk (Figs. 1b and 9), and at 20 km west of Aydın (Figs. 1b and 10).
365 Similar to the previous geothermal systems, both Salavatlı and Germencik geothermal systems
366 are located close to the Büyük Menderes detachment (Fig. 1b). Even though the age of top-to-the-
367 north ductile deformation is still controversial (*e.g.* Bozkurt 2001; Gessner *et al.* 2001a; Seyitoglu
368 and Işık 2015), all studies indicate a second top-to-the-south ductile-brittle shearing event (*e.g.*
369 Hetzel *et al.* 1995a; 1995b; Gessner *et al.* 2001b; Bozkurt and Sözbilir 2004).

370 In details, the geological sequence of the Salavatlı geothermal field is composed of Neogene
371 sediments deposited over schist-marble sequences and augen gneiss unit (Fig. 9a). Even though
372 the major structural feature does not clearly outcrop in this area due to strong neo-tectonic
373 overprint, the Büyük Menderes detachment was identified in two different drill holes

374 (Karamanderesi and Helvaci 2003). According to this study, the marble sequences in the
375 Menderes massif at ~ 800 m depth host the main geothermal reservoirs. Our new field
376 observations suggest that the general structure and the topography are mainly induced by a set of
377 major normal- to strike-slip faults. These faults control the first-order distribution of lithologies
378 of the two main units (augen gneiss and schist-marble sequences, Fig. 9a). The first ones are NW-
379 SE trending faults with opposite dips (Figs. 9b and 9c), showing kinematic indicators of a normal
380 movement. Here, kinematic indicators are compatible with a top-to-SW motion. The second ones
381 are the most important and they strike N-S to NE-SW (Fig. 9c). Locally, slickenlines are well
382 preserved and indicate a sinistral movement. These high-angle faults are characterized by a thick
383 fault gouge and crosscut all earlier structures, such as NW-SE trending faults, and also the
384 detachment (see the profile of Karamanderesi and Helvaci 2003). Close to these main structures,
385 hot springs are often observed (Fig. 9a), suggesting a first-order control on the emergence of
386 thermal fluids. In addition, the presence of N-S to NE-SW trending travertine deposits in higher
387 altitudes (Karamanderesi and Helvaci 2003) confirm the key role of such structures.

388 The Germencik geothermal field is characterized by numerous fumaroles, hot springs,
389 travertines and widespread hydrothermal alterations (*e.g.* Çamurlu and Bozköy hot springs; Fig.
390 10a). The Menderes basement rocks are mainly composed of Paleozoic metamorphic rocks such
391 as the augen gneiss and schist-marble sequences, overlain by Neogene sediments. North of
392 Çamurlu hot spring (Fig. 10a), the main foliation of metamorphic units strikes E-W and the
393 Neogene sediments dip slightly toward the north (Fig. 10a). Locally, travertines are located close
394 to this contact (Fig. 10a), showing that it acts as a major drain for fluid circulation. In addition, in
395 the vicinity of Bozköy, the main foliation of metamorphic units strikes NW-SE with a low dip
396 values (~ 5 – 10°) (Fig. 10b), whereas the Neogene sediments dips to the south (Fig. 10c). Such
397 an unexpected change of dip direction may suggest a fault drag area and the possible presence of
398 a N-S high-angle strike-slip transfer fault (Fig. 10a). Here again, the occurrence of geothermal

399 surface expressions suggests that this type of faults favours fluid circulation (Fig. 10d). More
400 recent tectonic features are also well expressed and consist in the development of E-W striking
401 high-angle normal faults (Figs. 10a and 10f). Some of them are characterized by dip values
402 (reaching $\sim 60^\circ$; Fig. 10e). When such faults root in the Büyük Menderes detachment at depth
403 (Fig. 10e), others dip steeper ($\sim 80^\circ$) and crosscut it. This latter set of faults has allowed for
404 instance the exhumation of the Kızılcagedik Horst. This area is also characterized by numerous
405 deep wells (see location of Ömerbeyli in Fig. 10a), and the highest temperatures were reached in
406 the Büyük Menderes graben ($\sim 230^\circ\text{C}$ at a depth of 975 m and 1196 m; Filiz *et al.* 2000). Here,
407 the E-W trending high-angle faults generate a wide fractured zone.

408

409 4.4. Structural features of the Seferihisar geothermal field

410 The Seferihisar geothermal field (Table 1 for more information) is located in the northern
411 flank of the Büyük Menderes graben between Sultanhisar and Köşk (Figs. 1b and 11a). The
412 basement of the Menderes Massif in this area is made of metamorphic rocks such as schists,
413 marbles and local phyllite intercalations (*e.g.* Dora *et al.* 1990; Güngör and Erdoğan 2002) topped
414 by the Bornova flysch mélangé. This area is similar to the central part of the Menderes Massif,
415 but shows some differences such as lower topography and a hidden tectonic contact localized
416 between the Bornova flysch mélangé and the Menderes Massif as suggested by Erdoğan (1990).
417 We briefly present below the relationships between hot spring locations and faults, and we refer
418 the reader to the study of Ring *et al.* (2017) for more information about the Miocene-to-Present
419 tectonic evolution. Field observations show that hot springs are generally located close to NE to
420 SW striking strike-slip faults (Figs. 11a, 11b and 11c). Kinematic indicators suggest a dextral
421 strike-slip movement with lineation pitch ranging from 10°S to 22°S (Fig. 11d). In addition, these
422 faults are characterized by multi-metric damaged zones, locally strongly altered, attesting for
423 recent fluid circulation. Dextral strike-slip movement is associated with dilational jogs and pull-

424 apart structures (Fig. 11a), probably close to the intersection zones between N-S strike-slip fault
425 and the early contact between the Bornova mélangé and the Menderes basement rocks (*i.e.* the
426 tectonic contact described by Erdoğan (1990)). Furthermore, in places, E-W trending fault
427 corridors cut these first faults (Fig. 11e). These later sub-vertical faults show several sub-vertical
428 and sub-horizontal slickenlines, with plunging values ranging from 85°W to 49°E and 24°E to
429 4°W, respectively (Fig. 11e). The calculated paleo-stress analysis suggests that kinematic
430 indicators are compatible with a NW-SE extension (Fig. 11a). All along the main road between
431 Cumhuriyet and Orhanlı (Fig. 11a), sandstones of Bornova mélangé usually display a strong
432 alteration. Hence, it seems reasonable to assume the existence of others faults, which would be
433 parallel to the previous one in this area.

434

435 **5. Discussion**

436 5.1. The Menderes Massif Core complex and associated geothermal fields

437 The genesis of a geothermal system requires source of high temperatures, reservoirs of large
438 quantity of hot fluids (permeable structures and lithology) and its caprock. All of these features
439 are present in the Menderes Massif, thus explaining the geothermal potential. As seen previously,
440 thermal anomalies show different wavelengths at different depths in the Menderes Massif (*i.e.*
441 crustal-scale to geothermal field-scale). Whereas the short wavelength anomalies result from
442 shallow depth processes and may be associated with N-S transfer faults, the long wavelength (*i.e.*
443 crustal-scale or mantle-scale) result from deep processes and may be associated with detachments
444 activity. Therefore, as for many geothermal fields in western Turkey and abroad, faults appear to
445 represent a first-order control on fluid flow and heat transport, and thus on the location of
446 reservoirs at depth and hot springs at the surface as leak of reservoir (Fig. 12a). In the following,
447 we first focus on detachments at crustal-scale, then we highlight the role of N-S transfer faults at
448 basin-scale.

449

450 5.1.1. Crustal-scale: the role of detachments

451 At the scale of the Menderes Massif, the presence at the surface of numerous hot springs
452 close to E-W striking, northward and/or southward dipping low-angle normal fault (Fig. 1b)
453 suggests that detachments control fluid circulations. These latter are controlled by the current
454 global structure of the Menderes core complex resulting from a multi-staged activity of the
455 detachments since the Miocene. Indeed, ongoing tectonic lets the detachment systems active, and
456 meanwhile, (i) detachment faults became incrementally split into many sections separated by
457 transfer faults and (ii) different sets of faults (*i.e.* E-W striking faults) merge at depth into the
458 detachments (see Seyitoglu *et al.* 2002). This complex tectonic evolution may induce an intense
459 hydrothermal activity (*e.g.* silicified detachment in some areas), for instance within thick damage
460 zone (*e.g.* up to 10 m of cataclasites associated with the Alaşehir detachment are present in the
461 hanging-wall and the footwall of the detachment, Fig. 7) reaching ~ 10 km (containing the ductile-
462 brittle deformation associated with the detachment) according to Bozkurt (2001). One can
463 question whether such detachment fault systems have acted as important conduits for fluid
464 circulations since the Miocene. In any case, these structures generate zones of high fracture
465 density and permeability that channel and host significant fluid flows in the upper crust. They are
466 also connected with most superficial structures (*i.e.* N-S transfer faults) and probably seem highly
467 effective for heat transport and fluid circulation at deeper depth toward specific reservoirs (Figs.
468 12a and 12b).

469 Many studies on fluid compositions (Famin *et al.* 2004; Mulch *et al.* 2007; Gottardi *et al.*
470 2011; Hetzel *et al.* 2013; Quilichini *et al.* 2015) suggest that low-angle detachments permit
471 pervasive meteoric fluid flow downward and/or upward along detachment fault planes, reaching
472 depths of 10 – 15 km. In addition, isotopic studies show the presence of small amounts of deep
473 CO₂, H₂S, B and He in thermal waters (see our compilation, section 3.2). We thus suggest that
474 large-scale detachment faults may represent the conduits allowing the escape of helium to the

475 surface in the Menderes Massif. In others words, fault-controlled circulation of meteoric fluids is
476 the dominant mechanism to explain the migration of mantle volatiles from the ductile-brittle
477 transition zone to the near-surface (Fig. 12b) (Mutlu *et al.* 2008; Jolie *et al.* 2016). Brittle fault
478 systems are thus probably connected at depth with ductile shear zones (Fig. 12b).

479 Ductile shear zones may indeed represent efficient pathways for hydrothermal fluids (*e.g.*
480 Oliver, 1996; Taillefer *et al.* 2017). Two main mechanisms explain the fluid migration in the
481 deeper part of the crust: deformation-driven flow (Oliver, 1996) and thermally-driven flow (*i.e.*
482 buoyancy-driven) through the crust, which is favoured by the high (i) permeability of detachments
483 that collect and bring up deep hot fluids and (ii) temperature induced by the shear heating
484 mechanism. This latter term refers to the generation of heat from the mechanical work of tectonic
485 processes (Scholz 1980). It thus increases with slip rate, friction coefficient and stiffness of
486 materials (Leloup *et al.* 1999; Souche *et al.* 2013). Considered as a most rapidly deforming regions
487 (*e.g.* Reilinger *et al.* 2006), western Anatolia domain would favour the development of such
488 mechanism at crustal-scale. Indeed, neo-tectonic activity in the Menderes Massif is characterized
489 by earthquakes occurring in the shallow crust, with the mean depth being shallower in the Simav
490 domain (9.7 km) compared to the western domain (11.9 km) and the central Menderes (11.2 km)
491 domain (Gessner *et al.* 2013). Brittle deformation is still active (*e.g.* the Gediz detachment,
492 Buscher *et al.* (2013)) and may locally occur under high temperatures conditions (*e.g.* 580 °C at
493 ~ 10 km, Bilim *et al.* 2016), probably close to the ductile-brittle transition zone. The numerous
494 ductile shear zones may have had (and perhaps still have; *e.g.* Ring *et al.* 2017) a strong and
495 continuous thermal effect at depth, explaining also the anomalously shallow position of Curie-
496 point depths. Hence, in these areas heat could also be generated by tectonic processes, probably
497 along the brittle-ductile shear zones in the upper levels of the continental crust (Fig. 12b) (Scholz
498 1980). Although the contribution of shear heating at crustal scale is debated (Lachenbruch and

499 Sass 1992), more studies would be needed to explore this possibility. In particular, the amount of
500 heat produced and the time constants of such heat production should be addressed.

501 Furthermore, using a numerical model of coupled fluid flow and heat transport processes,
502 Magri *et al.* (2010) showed that temperature patterns in the Seferihisar-Balçova area result from
503 both interaction of convective flow (*i.e.* buoyancy-driven flow) and meteoric recharge induced by
504 the horst (*i.e.* mixed convection) in the shallower crust. Recently, Roche *et al.* (2018) showed that
505 high temperatures at 6 km depth (300 – 350 °C) are sufficient to allow a high fluid density contrast,
506 permitting upward flow along the low-angle fault, using also 2-D numerical models (see Fig. 8 in
507 their study). This implies that buoyancy-driven flow is superimposed to topography-driven flow
508 in some places. This case is, for instance, well observed in the Seferihisar geothermal systems
509 where the topographic gradient related to the formation of MCC appears to be negligible. This
510 implies that the observed temperature patterns result mainly from the thermally driven flow within
511 permeable faults. In all cases, hot fluids in the detachments will further enhance temperature
512 increase in the upper part of the fault zone, thus generating high thermal gradients in these areas.
513 For instance, Gottardi *et al.* (2011) estimated high temperature gradient of ~140 °C/100 m across
514 the Miocene Raft River shear zone in the United States, as revealed by isotope thermometry.
515 There, the geotherm is quasi-stable over a long time duration. As a consequence, it raises the
516 question whether similar geothermal fields in the Menderes Massif could have been active during
517 millions of years.

518 Additionally, it is clear that permeability related to fault zones architecture is a first-order
519 control on fluid flow in the upper crust (*e.g.* Caine *et al.* 1996). Our study shows that the thick
520 siliceous microbreccia of the Alaşehir detachment fault plane (Table 2) acts as cap fault of the
521 fluid circulating below this plane. Thus, depending on the area, the detachment can be considered
522 at kilometric-scale as a combined “conduit-barrier” and as a “localized conduit” (Caine *et al.*
523 1996), where the conduit corresponds to the thick shear zone and the barrier is associated with the

524 fault plane and/or with the hanging wall of the detachment. Depending on the pressure gradients,
525 the flow within the detachment may be characterized by horizontal-flow according to normal
526 kinematic and related dilatancy (Fig. 12a). In both cases, the high permeability in the shear zone
527 favours fluid circulation (*e.g.* in marbles levels through karstification process in the Menderes
528 Massif) and thus generates secondary reservoirs (Fig. 12a).

529

530 5.1.2. Basin-scale: the N-S transfer faults

531 Based on our structural observations, we highlight that strike-slip faults control many
532 geothermal reservoirs in depth, related to hot springs and travertine deposits at the surface. In
533 terms of geometry, for instance, Çiftçi and Bozkurt (2010) suggested, from a seismic profile
534 interpretation, the existence of two kilometric transfer faults with a large normal component in
535 the Alaşehir graben (Fig. 4a). These transfer faults correspond to the location of several travertines
536 oriented NW-SE and NE-SW and hot springs at the surface, which are respectively associated
537 with the Urganlı (Temiz and Eikenberg 2011) and Alaşehir geothermal field (Fig. 4a). Kaya
538 (2015) also suggests that the Tekkehamam geothermal field (located in the southern part of the
539 Büyük Menderes graben, Fig. 1b) is associated with a N-S transfer fault that cuts both the
540 basement and Neogene sediments. Thus, this set of faults is a good candidate to act as conduit for
541 fluid circulation when hot springs and related travertines are located far from the detachment (Fig.
542 12a; Table 2). Here, horse-tail termination of these strike-slip faults (see more details in Faulds *et*
543 *al.* 2011), generates many closely spaced faults that locally increase permeability, favouring the
544 growth of reservoirs.

545 Although no clear chronology between detachments and the N-S strike-slip transfer zones
546 can be observed in the field, we favour a contemporaneous and ongoing development of these
547 faults systems during the development of the sedimentary basin according to Oner and Dilek
548 (2013). They are mainly found at the foothills of the main Menderes mountains, crosscutting the

549 detachments in high topographic zones. Nonetheless, we suggest that these faults may also root
550 to detachments at deeper depth (Fig. 12a). There, pull-apart structures, *en échelon* and relay-ramp
551 faults may be locally developed, generating dilational jogs with vertical pitch that focus fluid
552 circulation and thus geothermal upflow (Fig. 6d and Fig. 11c). In addition, reservoirs are
553 commonly focused at the dilational junction between detachments and nearby N-S strike-slip
554 faults or within the strike-slip faults (*e.g.* Cumalı fault, Figs. 11a and 12a).

555 To sum-up, these faults define several hundred meters wide relay zones where faults are
556 considered as “distributed conduits” (Caine *et al.* 1996). They are characterized by multiple minor
557 faults, connected with major structures where fluids can flow through highly fractured
558 metamorphic rocks thanks to the seismic pumping mechanism (*e.g.* Sibson *et al.* 1975; McCaig
559 1988; Famin *et al.* 2005). Consequently, we refer hereafter to these sinistral or dextral strike-slip
560 faults as the “geothermal transverse and transfer faults” related to main reservoirs (Fig. 12a).
561 Hence, these faults should be used as a main guide for geothermal exploration. This hypothesis is
562 opposed to the idea of Gessner *et al.* (2017), suggesting that NNE-SSW-orientated lineaments do
563 not have a significant role in fluid flow pattern.

564

565 5.2. Possible fluid pathways in the Menderes Massif: from the mantle to the geothermal 566 reservoir

567 In this study we have emphasized two types of control on hot springs and related geothermal
568 fluid flow in the Alaşehir, Büyük Menderes and Cumaovası basins: a structural control and a
569 lithological control (Table 2), which is also determinant to understand the location of hot springs
570 and to explain the position of reservoirs at depth. In the following, we first propose a fluid pathway
571 at the scale of the Menderes Massif (Fig. 12a) and then we mention a possible long-live duration
572 for this type of systems.

573

574 5.2.1. Source to sink

575 Based on structural analyses of field data and isotopic distribution of waters, we suggest
576 similar pathways of fluids for the Alaşehir and the Büyük Menderes half-grabens, that could also
577 extend to the Simav graben and Cumaovası basin: meteoric cold waters and/or sea waters (*i.e.* for
578 the Seferehisar case) circulate downwards along E-W high-angle to listric normal faults (*e.g.*
579 Salihli and Alaşehir geothermal systems), implying that such faults control the meteoric recharge
580 of deeper reservoirs (Fig. 12a). More generally, meteoric water infiltration along fractured rocks
581 of the basement of the Menderes Massif is controlled by (i) the footwall topography gradient
582 induced by MCC exhumation, and by (ii) the stress regime in the crust, allowing recharge and
583 hydrothermal fluid circulation. Then, temperature of fluids increases progressively. Hot fluids can
584 circulate along the main detachments (*i.e.* Simav, Alaşehir and Büyük Menderes detachments)
585 related to karstified marbles or/in fractured rocks of the basement. During this stage, the
586 geochemical properties of meteoric waters are modified and their composition (*e.g.* Na-HCO₃
587 type) is mainly controlled by calcite dissolution in the marbles layers of the Menderes Massif
588 under high temperature conditions. Locally, some exchange with mantle-He, CO₂, B and H₂S
589 isotopes could occur in deep parts of the crust in the ductile-brittle transition zone (Fig. 12b).
590 Through a seismic pumping mechanism (*e.g.* Sibson *et al.* 1975; McCaig 1988; Famin *et al.* 2005),
591 hydraulic gradients may force fluid downward across the ductile-brittle transition using the high
592 permeability of microcrack networks (*e.g.* after earthquake rupture). After a complex deep fluid
593 pathway, thermal waters may then recharge reservoirs of the metamorphic rocks of the Menderes
594 at depth (Figs. 12a and 12b).

595 Different lithologies may behave as reservoirs (Table 1). Reservoirs are herein defined by
596 highly fractured but also by karstified carbonate layers of the CMM (*e.g.* Salihli, Alaşehir,
597 Germencik, Salavatlı...; Tarcan *et al.* 2000). For instance, the high-temperature geothermal
598 reservoir observed in Alaşehir, is located in the upper section of the Paleozoic basement, with

599 feeder zones in the upper Paleozoic carbonates at approximately 1150 m and 1600 m of depth
600 (Akin *et al.* 2015). Fractured metamorphic rocks such as quartzite can also act as an aquifer for
601 geothermal fluid (e.g., Kızıldere; Simsek 2003). In both cases, the main reservoirs are located just
602 below the detachments, which is in some places silicified (Fig. 12a). There, blind geothermal
603 reservoirs may also form. Indeed, according to Magri *et al.* (2010), when hydrothermal plumes
604 reach the upper impermeable boundary (e.g. the Alaşehir detachment), over-pressured blind
605 geothermal reservoirs are formed. This implies that other geothermal systems in the Menderes
606 Massif are yet to be discovered. In order to fully understand these geothermal systems, stress
607 modelling related to faulting is necessary to bring new constraints on the evolution of fluid
608 pathways (Moeck *et al.* 2009). In addition, other reservoir types may be developed in the hanging-
609 wall of detachments. For example, in the Cumaovası basin, it is made of fractured submarine
610 volcanics of the Bornova mélange (Tarcan and Gemici 2003). Because of the high permeability
611 units in Neogene continental silicoclastic rocks, secondary aquifers may also occur (Fig. 12a).
612 Indeed, Neogene sediments may have highly variable permeability, but they usually rather display
613 mega-cap rocks related to underlying geothermal system (Tarcan *et al.* 2000; e.g. the Alaşehir
614 geothermal system).

615 After a short time of residence (around 20 – 50 years, Simsek 2003) in different kinds of
616 reservoirs, hot thermal fluids can flow along the dilational intersections or junction between the
617 N-S strike-slip faults and the detachment, and then emerge at the surface (e.g. Kurşunlu, Sart-
618 Çamur, Germencik hot springs) (Fig. 12a). In this case, the direction of flow is mainly determined
619 by the prevailing permeability and by the regional stress field. Similar features of fluid flow
620 pattern are observed in the Cumaovası basin where the NE-SW trending strike-slip faults affected
621 also the detachment, forming dilational jogs and favouring hot water circulation from karstic and
622 fractured reservoirs to the surface (e.g. Figs. 11b and 11c).

623

624 5.2.2. A long-lived duration geothermal Province?

625 Hetzel *et al.* (2013) suggested that the Alaşehir and Büyük Menderes detachments recorded
626 a long-lived brittle deformation from around 22 Ma until 4 – 3 Ma. Hence, the low-angle crustal
627 normal faults were (still) active over a long period of time. We thus suggest that detachments
628 controlled magma ascent (*e.g.* Salihli granodiorite, Egrigöz granite) as well as fluid circulation in
629 the Menderes Massif during the Miocene. Nonetheless, the presence of Kursunlu Sb-Hg(-Au)
630 deposit (Larson and Erler 1993) located within the Alaşehir detachment system, implies a drastic
631 change in the fluid pathway evolution compare to the Miocene. Indeed, according to Larson and
632 Erler (1993), Alaşehir detachment conveyed deep circulation of shallow hydrothermal fluids (*i.e.*
633 meteoric origin) with a minor component of crustal and mantellic origin, thus similar to the
634 present-day hot springs. Hence, the mineralizing fluid seems to be not related to the Miocene
635 intrusions. To better characterize this evolution, a detailed study of such deposit would be useful,
636 bringing new constraints on the structural control of the mineralization and the timing of
637 mineralizing processes. This imply that detachments control fluid pathways over millions years
638 (episodic or continuous mineralized pulse(s)?).

639

640 5.3. Origin of heat source in the Menderes Massif

641 At geodynamic-scale, the origin of the thermal anomalies propagating all the way to the
642 surface could reflect both slab-rollback and slab tear below western Turkey. Heat can be generated
643 by many processes, including anomalous mantle heat flow mainly due to asthenospheric flow and
644 shear heating (Fig. 12c) (Roche *et al.* 2018). Based on heat conduction, the time scale t_{diff} is
645 defined by the following equation:

$$646 t_{diff} = L^2 / \kappa \quad (1)$$

647 where L is Moho depth (meter) and κ is the thermal diffusivity ($m^2 s^{-1}$). Considering a Moho depth
648 of ~ 25 km under the Menderes Massif (*e.g.* Karabulut *et al.* 2013) and taking a thermal diffusivity

649 (κ) of $10^{-6} \text{ m}^2 \text{ s}^{-1}$, the current thermal anomaly observed at the surface (shown by the presence of
650 numerous sources and gas events) could reflect the thermal expression of a 20 Ma old slab tear at
651 Moho depth. In other words, the heat source at the base of the crust coupled to the exhumation of
652 the MCC is induced by slab dynamics since the Miocene as suggested by previous authors (*e.g.*
653 Jolivet *et al.* 2015; Menant *et al.* 2016; 2018; Roche *et al.* 2018). This increase of temperature
654 recorded in the mantle and in the crust favours the emplacement of a large zone of migmatization
655 and/or magmatic underplating at the base of the crust. This hypothesis is also consistent with:

- 656 (i) the presence of high temperatures ($\sim 580 \text{ }^\circ\text{C}$) at shallow depths ($\sim 10 \text{ km}$ under the
657 Menderes; Aydin *et al.* 2005; Bilim *et al.* 2016);
- 658 (ii) the current models of Miocene slab tearing in this region (Jolivet *et al.* 2015).
- 659 (iii) the enrichment of mantle-He (Mutlu *et al.* 2008), B and sometimes high content of
660 CO_2 and H_2S within all thermal waters (Vengosh *et al.* 2002); for instance, mantle-
661 He values suggest that helium is probably transferred to the lower crust by degassed
662 fluids from deep mantle melts (Mutlu *et al.* 2008); these values comparable to that
663 observed in hydrothermal fluids from the western part of the Basin & Range
664 Province (4 – 25% mantle-He) where active volcanism is also absent (Kennedy and
665 Soest 2007).

666 To sum-up, the lack of significant magmatic activity in this area shows that the upper crust
667 and related magmatic bodies is not a direct heat source for these geothermal systems (Faulds *et*
668 *al.* 2010). Nevertheless, based on 3-D Vp imaging of the upper crust beneath the Denizli
669 geothermal field, Kaypak and Gökkaya (2012) showed that intrusive magmatic bodies may also
670 explain the heat source of few geothermal systems in this area. According to this study and others
671 (*e.g.* Faulds *et al.* 2010; Kaya 2015; Gessner *et al.* 2017) the spatial distribution of hot springs and
672 fumaroles is associated with the tectonic activity. Using the classification of Moeck (2014), the
673 “geothermal Province” of the Menderes Massif can be considered as a fault controlled system in

674 an extensional domain, where convection occurs along the transfer fault systems. Although most
675 of existing models of geothermal heat source suggest a probable magmatic intrusion in the upper
676 crust, this study argues that the tectonic activity induced by subduction dynamics controls the
677 spatial distribution of heat in the Menderes massif (Fig. 12c) (*e.g.* Kaya 2015; Gessner *et al.* 2017;
678 Roche *et al.* 2018). We thus think that this area may be used as a reference case to better
679 understand the amagmatic geothermal systems/Provinces.

680

681 5.4. An underestimated geothermal potential?

682 It is clear that dense fracturing caused by tectonic activity implies a modification of the
683 regional fluid flow, which is controlled by the state of stress in the crust, and influences the
684 localisation and the typology of reservoirs. Reilinger *et al.* (2006) have estimated fault-slip rates
685 in a block model consisting of 19 plates/blocks and using $M > 4.5$ earthquakes above 35 km. Based
686 on GPS-derived velocity field data, they suggested a total extension of approximately 25 mm/yr
687 corresponding to 10.9 ± 0.3 mm/yr for the left lateral strike-slip component and 14.5 ± 0.3 mm/yr
688 of pure extension. This rapid relative motion is twice the rate reported from the Basin & Range
689 Province where Bennett *et al.* (2003) estimate relative motion of 9.3 ± 0.2 mm/yr with high strain
690 rates, using the same method (*i.e.* GPS-derived velocity field data). Faulds *et al.* (2012) showed
691 that the regional pattern of geothermal activity in the same area is directly correlated with strain
692 rates. If we compare, for instance, the total discharge of the Seferihisar geothermal field (*e.g.* 100
693 – 150 L/s to 300 L/s according to Tarcan and Gemici (2003)), located in a seismically active zone
694 (*e.g.* see compilation from Özkaymak *et al.* 2013) is twice to four times that of the Salihli
695 geothermal field (2 – 80 l/s; Özen *et al.* 2012), which is a less active zone. Paradoxically, the
696 topography is less steep in Seferihisar area than in Salihli area. Therefore, we suggest that active
697 deformation could affect fluid velocity in the upper crust, improving the flow rates of a geothermal
698 system.

699 Furthermore, the Basin & Range Province is quite similar to the Menderes Province because
700 MCCs are exhumed along low-angle normal faults, and represent a favourable setting for
701 amagmatic high enthalpy geothermal resources (Roche *et al.* 2018). In addition, the origin of the
702 heat of these systems may be also associated with a deeper source induced by subduction
703 dynamics (*i.e.* magmatic underplating under the overriding plate; Wannamaker *et al.* 2006).
704 Because of the similarities between these both geothermal Provinces, we suggest that the
705 geothermal potential in the Menderes is probably underestimated (~ 820 MWe, Geothermal
706 Resource Association estimated in 2018). Indeed, the current geothermal installed capacity of the
707 Basin & Range province is estimated at ~ 2349 MWe (Bertani, 2016).

708

709 **6. Conclusion**

710 Our work is based on a multiscale study and on a compilation of geothermal and structural
711 observations in the whole Menderes Massif. It provides a new vision on the role of a large-scale
712 thermal anomaly below the Menderes Massif and more generally in the Eastern Mediterranean
713 region. We suggest that such regional thermal anomalies at the origin of the Menderes geothermal
714 Province result from the tectono-thermal evolution of the Aegean subduction zone at depth. This
715 Province is characterized by an intense hydrothermal activity, favoured by both a high elevation
716 area and a neo-tectonic activity in absence of magmatic input. Such proxies are related to the
717 Menderes Core Complex evolution, which is structured by three main detachments. We also have
718 identified, at crustal-scale, the essential role of the low-angle normal faults, corresponding to a
719 permeable channelized fluid flow systems for ascending fluid flows. N-S transfer faults then
720 control the position of geothermal systems and should be used as a main guide for geothermal
721 exploration. In addition, we emphasize that the lithological control is determinant for
722 understanding the location of geothermal reservoirs, and may have a strong influence in the fluid
723 circulation pattern of thermal waters. Eventually, we highlight that an episodic model (*e.g.* seismic

724 pumping) and / or a continuous model seem possible over several million years in the Menderes
725 Massif.

726 **7. Acknowledgements:**

727 This work has received funding from the Labex Voltaire (ANR-10-LABX-100-01) homed at
728 Orléans University and BRGM, the French geological survey. The paper benefited from relevant
729 revisions by Inga Moeck, Klaus Gessner and Gürol Seyitoğlu. We also thank the Editor in chief,
730 Wolf-Christian Dullo.

731

732 **8. References:**

- 733 Akin, S., Yildirim, N., Yazman, M., Karadag, M., Seçkin, C., Tonguç, E., Gürel, E., Yarim, H.,
734 2015. Coiled Tubing Acid Stimulation of Alaşehir Geothermal Field, Turkey.
- 735 Akkus, I., Akıllı, H., Ceyhan, S., Dilemre, A., Tekin, Z., 2005. Türkiye jeotermal kaynakları
736 envanteri. MTA Genel Müdürlüğü Yayınları, Envanter Serisi, 201.
- 737 Alçiçek, H., Bülbül, A., Brogi, A., Liotta, D., Ruggieri, G., Capezzuoli, E., ..., Alçiçek, M. C.,
738 2018. Origin, evolution and geothermometry of the thermal waters in the Gölemezli
739 Geothermal Field, Denizli Basin (SW Anatolia, Turkey). *Journal of Volcanology and
740 Geothermal Research*, 349, 1-30.
- 741 Altinoğlu, F.F., Sari, M., Aydın, A., 2015. Detection of Lineaments in Denizli Basin of Western
742 Anatolia Region Using Bouguer Gravity Data. *Pure Appl. Geophys.* 172, 415–425.
- 743 Andritsos, N., Dalambakis, P., Arvanitis, A., Papachristou, M., Fytikas, M., 2015. Geothermal
744 developments in Greece–Country update 2010-2014. In *Proceedings World Geothermal
745 Congress 2015* (pp. 19-24).
- 746 Asti, 2016. A source-to-sink history of supradetachment Gediz Graben (W Turkey): from
747 exhumation of the Central Menderes Massif through the Gediz Detachment Fault to
748 sedimentation in the graben.
- 749 Aydın, İ., Karat, H. İ., Koçak, A., 2005. Curie-point depth map of Turkey. *Geophysical Journal
750 International*, 162(2), 633-640.
- 751 Baba, A., Bundschuh, J., Chandrasekharam, D. (Eds.), 2014. *Geothermal systems and energy
752 resources: Turkey and Greece*. CRC Press.
- 753 Baba, A., Şimşek, C., Gündüz, O., Elçi, A., Murathan, A., 2015. Hydrogeochemical Properties
754 of Geothermal Fluid and Its Effect on the Environment in Gediz Graben, Western Turkey.
- 755 Bayrak, M., Serpen, Ü., İlkışık, O.M., 2011. Two-dimensional resistivity imaging in the
756 Kızıldere geothermal field by MT and DC methods. *J. Volcanol. Geotherm. Res.* 204, 1–11.

757 Bayram, A. F., and Simsek, S., 2005. Hydrogeochemical and isotopic survey of Kütahya-Simav
758 geothermal field. In Proceedings of World Geothermal Congress, Antalya, Turkey (pp. 24-
759 29).

760 Bennett, R. A., Wernicke, B. P., Niemi, N. A., Friedrich, A. M., Davis, J. L., 2003.
761 Contemporary strain rates in the northern Basin and Range province from GPS data.
762 *Tectonics*, 22(2).

763 Benoit, D., 1999. Conceptual models of the Dixie Valley, Nevada geothermal field.
764 *Transactions-Geothermal Resources Council*, 505-512.

765 Bertani, R., 2016. Geothermal power generation in the world 2010–2014 update report.
766 *Geothermics* 60, 31–43.

767 Bilim, F., Akay, T., Aydemir, A., Kosaroglu, S., 2016. Curie point depth, heat-flow and
768 radiogenic heat production deduced from the spectral analysis of the aeromagnetic data for
769 geothermal investigation on the Menderes Massif and the Aegean Region, western Turkey.
770 *Geothermics*, 60, 44-57.

771 Biryol, C.B., Beck, S.L., Zandt, G., Özacar, A.A., 2011. Segmented African lithosphere beneath
772 the Anatolian region inferred from teleseismic P-wave tomography. *Geophys. J. Int.* 184,
773 1037–1057.

774 Blackwell, D. D., Golan, B., Benoit, D., 2000. Thermal regime in the Dixie Valley geothermal
775 system. *Geothermal Resources Council Transactions*, 24, 223-228.

776 Bonneau, M. and Kienast, J.R., 1982. Subduction, collision et schistes bleus: exemple de l'Égée,
777 Grèce. *Bull. Soc. géol. France*, 7: 785-791.

778 Bozkurt, E., 2000. Timing of Extension on the Büyük Menderes Graben, Western Turkey, and
779 Its Tectonic Implications. *Geol. Soc. Lond. Spec. Publ.* 173, 385–403.
780 doi:10.1144/GSL.SP.2000.173.01.18

781 Bozkurt, E., 2001. Late Alpine evolution of the central Menderes Massif, western Turkey. *Int. J.*
782 *Earth Sci.* 89, 728–744. doi:10.1007/s005310000141

783 Bozkurt, E., Oberhänsli, R., 2001. Menderes Massif (Western Turkey): structural, metamorphic
784 and magmatic evolution—a synthesis. *Int. J. Earth Sci.* 89, 679–708.

785 Bozkurt, E., Sözbilir, H., 2004. Tectonic evolution of the Gediz Graben: field evidence for an
786 episodic, two-stage extension in western Turkey. *Geol. Mag.* 141, 63–79.

787 Bozkurt, E., Satır, M., Buğdaycıoğlu, Ç., 2011. Surprisingly young Rb/Sr ages from the Simav
788 extensional detachment fault zone, northern Menderes Massif, Turkey. *J. Geodyn.* 52, 406–
789 431.

790 Buck, W. R., 1988. Flexural rotation of normal faults. *Tectonics*, 7(5), 959-973.

791 Bülbül, A., Özen, T., Tarcan, G., 2011. Hydrogeochemical and hydrogeological investigations
792 of thermal waters in the Alasehir-Kavaklidere area (Manisa-Turkey). *Afr. J. Biotechnol.* 10,
793 17223–17240.

794 Bunbury, J. M., Hall, L., Anderson, G. J., Stannard, A., 2001. The determination of fault
795 movement history from the interaction of local drainage with volcanic episodes. *Geological*
796 *Magazine*, 138(2), 185-192.

797 Buscher, J. T., Hampel, A., Hetzel, R., Dunkl, I., Glotzbach, C., Struffert, A., ..., Rätz, M., 2013.
798 Quantifying rates of detachment faulting and erosion in the central Menderes Massif
799 (western Turkey) by thermochronology and cosmogenic ¹⁰Be. *Journal of the Geological*
800 *Society*, 170(4), 669-683.

801 Caine, J. S., Evans, J. P., Forster, C. B., 1996. Fault zone architecture and permeability
802 structure. *Geology*, 24(11), 1025-1028.

803 Çifçi, G., Pamukçu, O., Çoruh, C., Çopur, S., Sözbilir, H., 2011. Shallow and deep structure of a
804 supradetachment basin based on geological, conventional deep seismic reflection sections
805 and gravity data in the Buyuk Menderes Graben, western Anatolia. *Surveys in Geophysics*,
806 32(3), 271-290.

807 Çiftçi, N. B., Bozkurt, E., 2009. Pattern of normal faulting in the Gediz Graben, SW Turkey.
808 *Tectonophysics*, 473(1-2), 234-260.

809 Çiftçi, N.B., Bozkurt, E., 2010. Structural evolution of the Gediz Graben, SW Turkey: temporal
810 and spatial variation of the graben basin. *Basin Res.* 22, 846–873.

811 Collins, A.S., Robertson, A.H.F., 1998. Processes of Late Cretaceous to Late Miocene episodic
812 thrust-sheet translation in the Lycian Taurides, SW Turkey.

813 De Boorder, H., Spakman, W., White, S. H., Wortel, M. J. R., 1998. Late Cenozoic
814 mineralization, orogenic collapse and slab detachment in the European Alpine Belt. *Earth*
815 *and Planetary Science Letters*, 164(3), 569-575.

816 Delvaux, D., Sperner, B., 2003. New aspects of tectonic stress inversion with reference to the
817 TENSOR program. *Geological Society, London, Special Publications*, 212(1), 75-100.

818 Demircioğlu, D., Ecevitoglu, B., and Seyitoğlu, G., 2010. Evidence of a rolling hinge
819 mechanism in the seismic records of the hydrocarbon-bearing Alaşehir graben, western
820 Turkey. *Petroleum Geoscience*, 16(2), 155-160.

821 Dercourt, J., Zonenshain, L.P., Ricou, L.E., Kuzmin, V.G., Le Pichon, X., Knipper, A.L.,
822 Grandjacquet, C., Sbertshikov, I.M., Geysant, J., Lepvrier, C., Pechersky, D.H., Boulin, J.,
823 Sibuet, J.C., Savostin, L.A., Sorokhtin, O., Westphal, M., Bazhenov, M.L., Lauer, J.P. and

824 Biju-Duval, B., 1986. Geological evolution of the Tethys belt from the Atlantic to the Pamir
825 since the Lias. *Tectonophysics*, 123: 241-315.

826 Dilek, Y., Altunkaynak, Ş., 2009. Geochemical and temporal evolution of Cenozoic magmatism
827 in western Turkey: mantle response to collision, slab break-off, and lithospheric tearing in
828 an orogenic belt. *Geol. Soc. Lond. Spec. Publ.* 311, 213–233.

829 Dolmaz, M. N., Ustaömer, T., Hisarlı, Z. M., Orbay, N., 2005. Curie point depth variations to
830 infer thermal structure of the crust at the African-Eurasian convergence zone, SW Turkey.
831 *Earth, planets and space*, 57(5), 373-383.

832 Dora, O.Ö., Kun, N., Candan, O., 1990. Metamorphic history and geotectonic evolution of the
833 Menderes Massif. *IIESCA Proc*2:102-115.

834 Drahor, M.G., Berge, M.A., 2006. Geophysical investigations of the Seferihisar geothermal
835 area, Western Anatolia, Turkey. *Geothermics* 35, 302–320..

836 Emre, T., 1992. Gediz grabeni'nin (Salihli-Alaflehir arası) jeolojisi. 45. *Türkiye Jeoloji*
837 *Kurultayı Bildiri Ozleri*, s.60.

838 Emre, T., Sözbilir, H., 1997. Field evidence for metamorphic core complex, detachment faulting
839 and accommodation faults in the Gediz and Büyük Menderes grabens, western Anatolia,
840 in: *International Earth Sciences Colloquium on the Aegean Region, İzmir-Güllük, Turkey.*
841 pp. 73–93.

842 Emre, T., Tavlan, M., Akkiraz, M.S., İsintek, İ., 2011. Stratigraphy, Sedimentology and
843 Palynology of the Neogene–Pleistocene (?) Rocks Around Akçaşehir-Tire-İzmir (Küçük
844 Menderes Graben, Western Anatolia). *Turk. J. Earth Sci.* 20, 27–56.

845 Endrun, B., Lebedev, S., Meier, T., Tirel, C., Friederich, W., 2011. Complex layered
846 deformation within the Aegean crust and mantle revealed by seismic anisotropy. *Nature*
847 *Geoscience*, 4(3), 203.

848 Epstein, S., Sharp, R. P., Gow, A. J., 1965. Six-year record of oxygen and hydrogen isotope
849 variations in South Pole firn. *Journal of Geophysical Research*, 70(8), 1809-1814.

850 Erdoğan, B., 1990. İzmir-Ankara Zonu'nun, İzmir ile Seferihisar arasındaki bölgede stratigrafik
851 özellikleri ve tektonik evrimi. *TPJD Bül.* 2, 1–20.

852 Erkan, K., 2014. Crustal heat flow measurements in western Anatolia from borehole equilibrium
853 temperatures. *Solid Earth Discuss.* 6, 403–426.

854 Erkan, K., 2015. Geothermal investigations in western Anatolia using equilibrium temperatures
855 from shallow boreholes. *Solid Earth*, 6(1), 103. Ersoy, E.Y., Helvacı, C., Palmer, M.R.,
856 2010. Mantle source characteristics and melting models for the early middle Miocene mafic
857 volcanism in Western Anatolia: implications for enrichment processes of mantle lithosphere

858 and origin of K-rich volcanism in postcollisional settings. *Journal of Volcanology and*
859 *Geothermal Research*, 198, 112–128.

860 Faccenna, C., Piromallo, C., Crespo-Blanc, A., Jolivet, L. and Rossetti, F., 2004. Lateral slab
861 deformation and the origin of the Western Mediterranean arcs. *Tectonics*, 23:
862 doi:10.1029/2002TC001488.

863 Faccenna, C., Bellier, O., Martinod, J., Piromallo, C., Regard, V., 2006. Slab detachment
864 beneath eastern Anatolia: A possible cause for the formation of the North Anatolian fault.
865 *Earth and Planetary Science Letters*, 242(1-2), 85-97.

866 Famin, V., Philippot, P., Jolivet, L., Agard, P., 2004. Evolution of hydrothermal regime along a
867 crustal shear zone, Tinos Island, Greece. *Tectonics* 23.

868 Famin, V., Hébert, R., Philippot, P., Jolivet, L., 2005. Ion probe and fluid inclusion evidences
869 for co-seismic fluid infiltration in a crustal detachment. *Contrib. Mineral. Petrol.*, 150(3):
870 354-367, DOI 10.1007/s00410-005-0031-x.

871 Faults, J. E., Coolbaugh, M., Blewitt, G., Henry, C. D., 2004. Why is Nevada in hot water?
872 Structural controls and tectonic model of geothermal systems in the northwestern Great
873 Basin. *Geothermal Resources Council Transactions*, 28, 649-654.

874 Faults, J., Coolbaugh, M., Bouchot, V., Moek, I., Oguz, K., 2010. Characterizing Structural
875 Controls of Geothermal Reservoirs in the Great Basin, USA, and Western Turkey:
876 Developing Successful Exploration Strategies in Extended Terranes. Presented at the World
877 Geothermal Congress 2010, p. 11 p.

878 Faults, J. E., Hinz, N. H., Coolbaugh, M. F., Cashman, P. H., Kratt, C., Dering, G., ...,
879 McLachlan, H., 2011. Assessment of favorable structural settings of geothermal systems in
880 the Great Basin, western USA. *Geothermal Resources Council Transactions*, 35, 777-783.

881 Faults, J. E., Hinz, N., Kreemer, C., Coolbaugh, M., 2012. Regional patterns of geothermal
882 activity in the Great Basin Region, Western USA: correlation with strain rates. *Geothermal*
883 *Resources Council Transactions*, 36, 897-902.

884 Filiz, S., Tarcan, G., Gemici, U., 2000. Geochemistry of the Germencik geothermal fields,
885 Turkey, in: *Proceedings of the World Geothermal Congress*. pp. 1115–1120.

886 Gemici, Ü., Tarcan, G., 2002. Hydrogeochemistry of the Simav geothermal field, western
887 Anatolia, Turkey. *Journal of Volcanology and Geothermal Research*, 116(3-4), 215-233.

888 Genç, C. Ş., Altunkaynak, Ş., Karacık, Z., Yazman, M., Yılmaz, Y., 2001. The Çubukludağ
889 graben, south of İzmir: its tectonic significance in the Neogene geological evolution of the
890 western Anatolia. *Geodinamica Acta*, 14(1-3), 45-55.

891 Gessner, K., Piazzolo, S., Güngör, T., Ring, U., Kröner, A., Passchier, C.W., 2001a. Tectonic
892 significance of deformation patterns in granitoid rocks of the Menderes nappes, Anatolide
893 belt, southwest Turkey. *Int. J. Earth Sci.* 89, 766–780.

894 Gessner, K., Ring, U., Johnson, C., Hetzel, R., Passchier, C.W., Güngör, T., 2001b. An active
895 bivergent rolling-hinge detachment system: Central Menderes metamorphic core complex
896 in western Turkey. *Geology* 29, 611–614.

897 Gessner, K., Gallardo, L. A., Markwitz, V., Ring, U., Thomson, S. N., 2013. What caused the
898 denudation of the Menderes Massif: Review of crustal evolution, lithosphere structure, and
899 dynamic topography in southwest Turkey. *Gondwana Research*, 24(1), 243-274.

900 Gessner, K., Markwitz, V., Güngör, T., 2017. Crustal fluid flow in hot continental extension:
901 tectonic framework of geothermal areas and mineral deposits in western Anatolia.
902 Geological Society, London, Special Publications, 453, SP453-7.

903 Gottardi, R., Teyssier, C., Mulch, A., Vennemann, T. W., Wells, M. L., 2011. Preservation of an
904 extreme transient geotherm in the Raft River detachment shear zone. *Geology*, 39(8), 759-
905 762.

906 Govers, R. and Wortel, M.J.R., 2005. Lithosphere tearing at STEP faults: Response to edges of
907 subduction zones. *Earth and Planet. Sci. Lett.*, 236 505– 523.

908 Govers, R. and Fichtner, A., 2016. Signature of slab fragmentation beneath Anatolia from full-
909 waveform tomography. *Earth and Planetary Science Letters* 450 10–19;
910 <http://dx.doi.org/10.1016/j.epsl.2016.06.014>.

911 Güleç, N., 1988. Helium-3 distribution in western Turkey. *Miner. Res Expl Bull* 108, 35–42.

912 Güleç, N., Hilton, D.R., 2006. Helium and heat distribution in western Anatolia, Turkey:
913 Relationship to active extension and volcanism. *Geol. Soc. Am. Spec. Pap.* 409, 305–319.

914 Güleç, N., Hilton, D.R., Mutlu, H., 2002. Helium isotope variations in Turkey: relationship to
915 tectonics, volcanism and recent seismic activities. *Chem. Geol.* 187, 129–142.

916 Güngör, T., & Erdoğan, B. (2002). Tectonic significance of mafic volcanic rocks in a Mesozoic
917 sequence of the Menderes Massif, West Turkey. *International Journal of Earth Sciences*,
918 91(3), 386-397.

919 Haizlip, J. R., Haklıdır, F. T., Garg, S. K., 2013. Comparison of Reservoir Conditions in High
920 Noncondensable Gas Geothermal Systems. In proceedings, 38th Workshop on Geothermal
921 Reservoir Engineering (pp. 11-13).

922 Haklıdır, F. T., Sengun, R., Haizlip, J. R., 2015. The Geochemistry of the Deep Reservoir Wells
923 in Kizildere (Denizli City) Geothermal Field (Turkey). *Geochemistry*, 19, 25.

924 Hetzel, R., Passchier, C.W., Ring, U., Dora, Ö.O., 1995a. Bivergent extension in orogenic belts:
925 the Menderes Massif (southwestern Turkey). *Geology* 23, 455–458.

926 Hetzel, R., Ring, U., Akal, C., Troesch, M., 1995b. Miocene NNE-directed extensional
927 unroofing in the Menderes Massif, southwestern Turkey. *J. Geol. Soc.* 152, 639–654.

928 Hetzel, R., Zwingmann, H., Mulch, A., Gessner, K., Akal, C., Hampel, A., Güngör, T.,
929 Petschick, R., Mikes, T., Wedin, F., 2013. Spatiotemporal evolution of brittle normal
930 faulting and fluid infiltration in detachment fault systems: A case study from the Menderes
931 Massif, western Turkey. *Tectonics* 32, 364–376.

932 Isik, V., Tekeli, O., Cemen, I., 1997. Mylonitic fabric development along a detachment surface
933 in northern Menderes massif, western Anatolia, Turkey. In *Geol. Soc. America, Abstracts
934 with Programs*.

935 Işık, V., Tekeli, O., 2001. Late orogenic crustal extension in the northern Menderes Massif
936 (western Turkey): evidence for metamorphic core complex formation. *Int. J. Earth Sci.* 89,
937 757–765.

938 Işık, V., Seyitoğlu, G., Cemen, I., 2003. Ductile–brittle transition along the Alaşehir detachment
939 fault and its structural relationship with the Simav detachment fault, Menderes Massif,
940 western Turkey. *Tectonophysics* 374, 1–18.

941 Isik, V., Tekeli, O., Seyitoglu, G., 2004. The $^{40}\text{Ar}/^{39}\text{Ar}$ age of extensional ductile deformation
942 and granitoid intrusion in the northern Menderes core complex: implications for the
943 initiation of extensional tectonics in western Turkey. *Journal of Asian Earth Sciences*,
944 23(4), 555-566.

945 Jolie, E., Klinkmueller, M., Moeck, I., Bruhn, D., 2016. Linking gas fluxes at Earth's surface
946 with fracture zones in an active geothermal field. *Geology*, G37412-1.

947 Jolivet, L., Faccenna, C., 2000. Mediterranean extension and the Africa-Eurasia collision.
948 *Tectonics* 19, 1095–1106. doi:10.1029/2000TC900018

949 Jolivet, L., Brun, J.P., 2010. Cenozoic geodynamic evolution of the Aegean. *Int J Earth Sci Geol
950 Rundsch* 99, 109–138. doi:10.1007/s00531-008-0366-4

951 Jolivet, L., Goffé, B., Monié, P.,
952 Truffert-Luxey, C., Patriat, M., Bonneau, M., 1996. Miocene detachment in Crete and
953 exhumation P-T-t paths of high-pressure metamorphic rocks. *Tectonics*, 15(6), 1129-1153.

954 Jolivet, L., Faccenna, C., Huet, B., Labrousse, L., Le Pourhiet, L., Lacombe, O., ..., Philippon,
955 M., 2013. Aegean tectonics: Strain localisation, slab tearing and trench retreat.
956 *Tectonophysics*, 597, 1-33.

957 Jolivet, L., Menant, A., Sternai, P., Rabillard, A., Arbaret, L., Augier, R., Laurent, V., Beaudoin,
958 A., Grasemann, B., Huet, B., Labrousse, L., Le Pourhiet., L., 2015. The geological signature

958 of a slab tear below the Aegean. *Tectonophysics*, 659, 166-182.
959 doi:10.1016/j.tecto.2015.08.004

960 Jongsma, D., 1974. Heat flow in the Aegean Sea. *Geophysical Journal International*, 37(3), 337-
961 346. Karabulut, H., A. Paul, T. Afacan Ergün, D. Hatzfeld, D. M. Childs, M. Aktar, 2013.
962 Long-wavelength undulations of the seismic Moho beneath the strongly stretched Western
963 Anatolia, *Geophys. J. Int.*, 194, 450–464; doi: 410.1093/gji/ggt1100.

964 Karakuş, H., 2015. Helium and carbon isotope composition of gas discharges in the Simav
965 Geothermal Field, Turkey: Implications for the heat source. *Geothermics*, 57, 213-223.

966 Karamanderesi, İ.H., 1997. Salihli-Caferbey (Manisa İli) jeotermal sahası potansiyelive
967 geleceği. *Dünya Enerji Konseyi Türk Milli Komitesi, Türkiye 7. Enerji Kongresi teknik*
968 *oturma bildirisi metinleri*, pp. 247–261 (in Turkish).

969 Karamanderesi, İ.H., 2013. Characteristics of Geothermal Reservoirs in Turkey. IGA Academy
970 Report 0102-2013.

971 Karamanderesi, İ.H., Helvacı, C., 2003. Geology and hydrothermal alteration of the Aydın-
972 Salavatlı geothermal field, western Anatolia, Turkey. *Turk. J. Earth Sci.* 12, 175–198.

973 Kaya, A., 2015. The effects of extensional structures on the heat transport mechanism: An
974 example from the Ortakçı geothermal field (Büyük Menderes Graben, SW Turkey). *J. Afr.*
975 *Earth Sci.* 108, 74–88.

976 Kaypak, B., Gökkaya, G., 2012. 3-D imaging of the upper crust beneath the Denizli geothermal
977 region by local earthquake tomography, western Turkey. *Journal of Volcanology and*
978 *Geothermal Research*, 211, 47-60.

979 Kennedy, B. M., Van Soest, M. C., 2007. Flow of mantle fluids through the ductile lower crust:
980 Helium isotope trends. *Science*, 318(5855), 1433-1436.

981 Kennedy, B. M., Kharaka, Y. K., Evans, W. C., Ellwood, A., DePaolo, D. J., Thordsen, J., ...,
982 Mariner, R. H., 1997. Mantle fluids in the San Andreas fault system, California. *Science*,
983 278(5341), 1278-1281.

984 Kent, E., Boulton, S. J., Stewart, I. S., Whittaker, A. C., Alçiçek, M. C., 2016. Geomorphic and
985 geological constraints on the active normal faulting of the Gediz (Alaşehir) Graben,
986 Western Turkey. *Journal of the Geological Society*, jgs2015-121.

987 Kindap, A., Kaya, T., Haklıdır, F.S.T., Bükülmez, A.A., 2010. Privatization of Kizildere
988 Geothermal Power Plant and New Approaches for Field and Plant, in: *Proceedings World*
989 *Geothermal Congress*.

990 Koçyiğit, A., Yusufoglu, H., Bozkurt, E., 1999. Discussion on evidence from the Gediz Graben
991 for episodic two-stage extension in western Turkey. *Journal of the Geological Society*,
992 London, 156, 1240-1242.

993 Koçyiğit, A., 2015. An overview on the main stratigraphic and structural features of a
994 geothermal area: the case of Nazilli-Buharkent section of the Büyük Menderes Graben, SW
995 Turkey. *Geodinamica Acta*, 27(2-3), 85-109.

996 Kose, R., 2007. Geothermal energy potential for power generation in Turkey: a case study in
997 Simav, Kutahya. *Renewable and Sustainable Energy Reviews*, 11(3), 497-511.

998 Kulongoski, J. T., Hilton, D. R., Izbicki, J. A., 2005. Source and movement of helium in the
999 eastern Morongo groundwater Basin: the influence of regional tectonics on crustal and
1000 mantle helium fluxes. *Geochimica et cosmochimica Acta*, 69(15), 3857-3872.

1001 Lachenbruch, A.H., Saas, J.H., 1992. Heat flow from Cajon Pass, fault strength, and tectonic
1002 implications. *J. Geophys. Res* 97, 4995-5015.

1003 Larson, L. T., Erler, Y. A., 1993. The epithermal lithogeochemical signature—a persistent
1004 characterization of precious metal mineralization at Kursunlu and Örencik, two prospects of
1005 very different geology in western Turkey. *Journal of Geochemical Exploration*, 47(1-3),
1006 321-331.

1007 Leloup, P.H., Ricard, Y., Battaglia, J., Lacassin, R., 1999. Shear heating in continental strike-
1008 slip shear zones: model and field examples. *Geophys. J. Int.* 136, 19–40.

1009 Maddy, D., Veldkamp, A., Demir, T., van Gorp, W., Wijbrans, J. R., van Hinsbergen, D. J. J.,
1010 ..., Stemerink, C., 2017. The Gediz River fluvial archive: A benchmark for Quaternary
1011 research in Western Anatolia. *Quaternary science reviews*, 166, 289-306.

1012 Magri, F., Akar, T., Gemici, U., Pekdeger, A., 2010. Deep geothermal groundwater flow in the
1013 Seferihisar–Balçova area, Turkey: results from transient numerical simulations of coupled
1014 fluid flow and heat transport processes. *Geofluids* 10, 388–405.

1015 Malinverno, A., Ryan, W.B.F., 1986. Extension in the Tyrrhenian Sea and shortening in the
1016 Apennines as result of arc migration driven by sinking of the lithosphere. *Tectonics* 5, 227–
1017 245. doi:10.1029/TC005i002p00227

1018 Marty, B., O'nions, R. K., Oxburgh, E. R., Martel, D., Lombardi, S., 1992. Helium isotopes in
1019 Alpine regions. *Tectonophysics*, 206(1), 71-78.

1020 McCaig, A. M., 1988. Deep fluid circulation in fault zones. *Geology*, 16(10), 867-870.

1021 Menant, A., Jolivet, L., Vrielynck, B., 2016. Kinematic reconstructions and magmatic evolution
1022 illuminating crustal and mantle dynamics of the eastern Mediterranean region since the late
1023 Cretaceous. *Tectonophysics*, 675, 103-140.

1024 Menant, A., Jolivet, L., Tuduri, J., Loiselet, C., Bertrand, G. and Guillou-Frottier, L., 2018. 3D
1025 subduction dynamics: A first-order parameter of the transition from copper- to gold-rich
1026 deposits in the eastern Mediterranean region. *Ore Geology Reviews*, 94: 118-135.

1027 Mendrinou, D., Choropanitis, I., Polyzou, O., Karytsas, C., 2010. Exploring for geothermal
1028 resources in Greece. *Geothermics* 39, 124–137.

1029 Moeck, I.S., 2014. Catalog of geothermal play types based on geologic controls. *Renewable and*
1030 *Sustainable Energy Reviews*, 37, 867–882.

1031 Moeck, I.S., Schandelmeier, H., Holl, G.H., 2009. The stress regime in a Rotliegend reservoir of
1032 the Northeast German Basin. *International Journal of Earth Sciences*, 98(7), 1643–1654.

1033 Mulch, A., Teyssier, C., Cosca, M. A., Chamberlain, C. P., 2007. Stable isotope paleoaltimetry
1034 of Eocene core complexes in the North American Cordillera. *Tectonics*, 26(4).

1035 Mutlu, H., Güleç, N., Hilton, D.R., 2008. Helium–carbon relationships in geothermal fluids of
1036 western Anatolia, Turkey. *Chem. Geol.* 247, 305–321.

1037 Oliver, N.H.S., 1996. Review and classification of structural controls on fluid flow during
1038 regional metamorphism. *J. Metamorph. Geol.* 14 (4), 477–492.

1039 O'Nions, R. K., Oxburgh, E. R., 1988. Helium, volatile fluxes and the development of
1040 continental crust. *Earth and Planetary Science Letters*, 90(3), 331-347.

1041 Oner, Z., Dilek, Y., 2011. Supradetachment basin evolution during continental extension: the
1042 Aegean province of western Anatolia, Turkey. *Geological Society of America Bulletin* 123,
1043 2115–2141. <http://dx.doi.org/10.1130/B30468.1>.

1044 Oner, Z., Dilek, Y., 2013. Fault kinematics in supradetachment basin formation, Menderes core
1045 complex of western Turkey. *Tectonophysics*, 608, 1394-1412.

1046 Ozdemir, A., Yasar, E., Cevik, G., 2017. An importance of the geological investigations in
1047 Kavaklıdere geothermal field (Turkey). *Geomechanics and Geophysics for Geo-Energy and*
1048 *Geo-Resources*, 3(1), 29-49.

1049 Özen, T., Bülbül, A., Tarcan, G., 2012. Reservoir and hydrogeochemical characterizations of
1050 geothermal fields in Salihli, Turkey. *J. Asian Earth Sci.* 60, 1–17.

1051 Özgür, N., 2002. Geochemical signature of the Kizildere geothermal field, western Anatolia,
1052 Turkey. *Int. Geol. Rev.* 44, 153–163.

1053 Özgür, N., Pekdeger, A., Wolf, M., Stichler, W., Seiler, K. P., Satir, M., 1998a.
1054 Hydrogeochemical and isotope geochemical features of the thermal waters of Kizildere,
1055 Salavatli, and Germencik in the rift zone of the Büyük Menderes, western Anatolia, Turkey:
1056 Preliminary studies. In *Proceedings of 9th International Symposium on Water-Rock*
1057 *Interaction, Taupo, New Zealand (Vol. 30, pp. 645-648).*

1058 Özgür, N., Vogel, M., Pekdeger, A., 1998b. A new type of hydrothermal alteration at the
1059 Kizildere geothermal field in the rift zone of the Büyük Menderes, western Anatolia,
1060 Turkey.

1061 Özgür, N., Karamenderesi, I. H., 2015. An update of the geothermal potential in the continental
1062 rift zone of the Büyük Menderes, Western Anatolia, Turkey. In Proceedings, Fortieth
1063 Workshop on Geothermal Reservoir Engineering Stanford University (pp. 26-28).

1064 Özkaymak, Ç., Sözbilir, H., Uzel, B., 2013. Neogene–Quaternary evolution of the Manisa
1065 Basin: Evidence for variation in the stress pattern of the İzmir-Balıkesir Transfer Zone,
1066 western Anatolia. *Journal of Geodynamics*, 65, 117-135.

1067 Pfister, M., Rybach, L., Simsek, S., 1998. Geothermal reconnaissance of the Marmara Sea
1068 region (NW Turkey): surface heat flow density in an area of active continental extension.
1069 *Tectonophysics, Heat Flow and the Structure of the Lithosphere - IV* 291, 77–89.
1070 doi:10.1016/S0040-1951(98)00032-8

1071 Pik, R., Marty, B., 2009. Helium isotopic signature of modern and fossil fluids associated with
1072 the Corinth rift fault zone (Greece): implication for fault connectivity in the lower crust.
1073 *Chemical Geology*, 266(1), 67-75.

1074 Piromallo, C., Morelli, A., 2003. P wave tomography of the mantle under the Alpine-
1075 Mediterranean area. *Journal of Geophysical Research: Solid Earth*, 108(B2).
1076 <https://doi.org/10.1029/2002JB001757>

1077 Prelević, D., Akal, C., Foley, S. F., Romer, R. L., Stracke, A., Van Den Bogaard, P., 2012.
1078 Ultrapotassic mafic rocks as geochemical proxies for post-collisional dynamics of
1079 orogenic lithospheric mantle: the case of southwestern Anatolia, Turkey. *Journal of*
1080 *Petrology*, 53(5), 1019-1055.

1081 Purvis, M., Robertson, A., 2005. Sedimentation of the Neogene–Recent Alaşehir (Gediz)
1082 continental graben system used to test alternative tectonic models for western (Aegean)
1083 Turkey. *Sediment. Geol.* 173, 373–408.

1084 Quilichini, A., Siebenaller, L., Nachlas, W. O., Teyssier, C., Vennemann, T. W., Heizler, M. T.,
1085 Mulch, A., 2015. Infiltration of meteoric fluids in an extensional detachment shear zone
1086 (Kettle dome, WA, USA): How quartz dynamic recrystallization relates to fluid-rock
1087 interaction. *Journal of Structural Geology*, 71, 71-85.

1088 Reilinger, R., McClusky, S., Vernant, P., Lawrence, S., Ergintav, S., Cakmak, R., Ozener, H.,
1089 Kadirov, F., Guliev, I., Stepanyan, R., Nadariya, M., Hahubia, G., Mahmoud, S., Sakr, K.,
1090 ArRajehi, A., Paradissis, D., Al-Aydrus, A., Prilepin, M., Guseva, T., Evren, E., Dmitrotsa,
1091 A., Filikov, S.V., Gomez, F., Al-Ghazzi, R., Karam, G., 2006. GPS constraints on

1092 continental deformation in the Africa-Arabia-Eurasia continental collision zone and
1093 implications for the dynamics of plate interactions. *J. Geophys. Res. Solid Earth* 111,
1094 B05411. doi:10.1029/2005JB004051

1095 Richardson-Bunbury, J. M., 1996. The Kula volcanic field, western Turkey: the development of
1096 a Holocene alkali basalt province and the adjacent normal-faulting graben. *Geological*
1097 *Magazine*, 133(3), 275-283.

1098 Ring, U., Gessner, K., Güngör, T., Passchier, C. W., 1999. The Menderes Massif of western
1099 Turkey and the Cycladic Massif in the Aegean—do they really correlate?. *Journal of the*
1100 *Geological Society*, 156(1), 3-6.

1101 Ring, U., Johnson, C., Hetzel, R., Gessner, K., 2003. Tectonic denudation of a Late Cretaceous–
1102 Tertiary collisional belt: regionally symmetric cooling patterns and their relation to
1103 extensional faults in the Anatolide belt of western Turkey. *Geol. Mag.* 140, 421–441.

1104 Ring, U., Glodny, J., Will, T., Thomson, S., 2010. The Hellenic subduction system: high-
1105 pressure metamorphism, exhumation, normal faulting, and large-scale extension. *Annual*
1106 *Review of Earth and Planetary Sciences*, 38, 45-76.

1107 Ring, U., Gessner, K., Thomson, S., 2017. Variations in fault-slip data and cooling history
1108 reveal corridor of heterogeneous backarc extension in the eastern Aegean Sea region.
1109 *Tectonophysics*, 700, 108-130.

1110 Roche, V., Guillou-Frottier, L., Jolivet, L., Loiselet, C., Bouchot, V., 2015. Subduction and slab
1111 tearing dynamics constrained by thermal anomalies in the Anatolia-Aegean region.
1112 *Geophysical Research Abstracts Vol. 17*, EGU2015-6882, 2015 EGU General Assembly
1113 2015.

1114 Roche, V., Sternai, P., Guillou-Frottier, L., Jolivet, L., Gerya, T., 2016. Location of eastern
1115 Mediterranean hot springs induced by mantle heat flow due to slab roll-back and tearing.
1116 *AGU*

1117 Roche, V., Sternai, P., Guillou-Frottier, L., Menant, A., Jolivet, L., Bouchot, V., Gerya, T.,
1118 2018. Emplacement of metamorphic core complexes and associated geothermal systems
1119 controlled by slab dynamics. *Earth and Planetary Science Letters*, 498, 322-333.

1120 Ross, H. E., Blakely, R. J., Zoback, M. D., 2006. Testing the use of aeromagnetic data for the
1121 determination of Curie depth in California. *Geophysics*, 71(5), L51-L59.

1122 Salaün, G., Pedersen, H.A., Paul, A., Farra, V., Karabulut, H., Hatzfeld, D., Papazachos, C.,
1123 Childs, D.M., Pequegnat, C., Team, S., others, 2012. High-resolution surface wave
1124 tomography beneath the Aegean-Anatolia region: constraints on upper-mantle structure.
1125 *Geophys. J. Int.* 190, 406–420.

1126 Schlinger, C. M., 1985. Magnetization of lower crust and interpretation of regional magnetic
1127 anomalies: Example from Lofoten and Vesterålen, Norway. *Journal of Geophysical*
1128 *Research: Solid Earth*, 90(B13), 11484-11504.

1129 Scholz, C.H., 1980. Shear heating and the state of stress on faults. *J. Geophys. Res. Solid Earth*
1130 85, 6174–6184.

1131 Seyitoglu, G., 1997. The Simav graben: an example of young EW trending structures in the Late
1132 Cenozoic extensional system of western Turkey. *Turkish Journal of Earth Sciences*, 6,
1133 135-141.

1134 Seyitoğlu, G., Scott, B., 1991. Late Cenozoic crustal extension and basin formation in west
1135 Turkey. *Geological Magazine*, 128(2), 155-166.

1136 Seyitoğlu, G., Scott, B. C., 1996. The cause of NS extensional tectonics in western Turkey:
1137 tectonic escape vs back-arc spreading vs orogenic collapse. *Journal of Geodynamics*, 22(1-
1138 2), 145-153.

1139 Seyitoğlu, G., Işık, V., 2015. Late cenozoic extensional tectonics in western anatolia:
1140 exhumation of the menderes core complex and formation of related basins. *Bulletin Of The*
1141 *Mineral Research and Exploration*, (151).

1142 Seyitoğlu, G., Scott, B. C., Rundle, C. C., 1992. Timing of Cenozoic extensional tectonics in
1143 west Turkey. *Journal of the Geological Society*, 149(4), 533-538.

1144 Seyitoglu, G., Tekeli, O., Çemen, I., Sen, S., Isik, V., 2002. The role of the flexural
1145 rotation/rolling hinge model in the tectonic evolution of the Alasehir graben, western
1146 Turkey. *Geol. Mag.* 139, 15–26.

1147 Seyitoğlu, G., Işık, V., Cemen, I., 2004. Complete Tertiary exhumation history of the Menderes
1148 massif, western Turkey: an alternative working hypothesis. *Terra Nova*, 16(6), 358-364.

1149 Seyitoğlu, G., Işık, V., Esat, K., 2014. A 3D model for the formation of turtleback surfaces: the
1150 Horzum Turtleback of western Turkey as a case study. *Turkish Journal of Earth Sciences*,
1151 23(5), 479-494.

1152 Seyitoğlu, G., Işık, V., 2015. Late Cenozoic extensional tectonics in western anatolia:
1153 exhumation of the Menderes Core Complex and formation of related basins. *Bulletin of the*
1154 *mineral research and exploration*, (151).

1155 Sheppard, S. M. F., 1977. The Cornubian batholith, SW England: D/H and 18O/16O studies of
1156 kaolinite and other alteration minerals. *Journal of the Geological Society*, 133(6), 573-591.

1157 Sheppard, S. M., 1981. Stable isotope geochemistry of fluids. *Physics and Chemistry of the*
1158 *Earth*, 13, 419-445.

- 1159 Shimizu, A., Sumino, H., Nagao, K., Notsu, K., Mitropoulos, P., 2005. Variation in noble gas
1160 isotopic composition of gas samples from the Aegean arc, Greece. *Journal of Volcanology*
1161 and *Geothermal Research*, 140(4), 321-339.
- 1162 Sibson, R. H., Moore, J. M. M., Rankin, A. H., 1975. Seismic pumping—a hydrothermal fluid
1163 transport mechanism. *Journal of the Geological Society*, 131(6), 653-659.
- 1164 Şimşek, Ş., 1984. Aydın-Germencik-Omerbeyli geothermal field of Turkey. In *Proc. of UN*
1165 *Seminar on Utilization of Geothermal Energy for Electric Power Production and Space*
1166 *Heating*.
- 1167 Simsek, S., 1985. Geothermal model of Denizli, Sarayköy-Buldan area. *Geothermics* 14, 393–
1168 417.
- 1169 Simsek, S., 2003. Hydrogeological and isotopic survey of geothermal fields in the Büyük
1170 Menderes graben, Turkey. *Geothermics* 32, 669–678.
- 1171 Simsek, S., Demir, A., 1991. Reservoir and cap rock characteristics of some geothermal fields in
1172 turkey and encountered problems based on lithology. *J. Geotherm. Res. Soc. Jpn.* 13, 191–
1173 204.
- 1174 Souche, A., Medvedev, S., Andersen, T.B., Dabrowski, M., 2013. Shear heating in extensional
1175 detachments: Implications for the thermal history of the Devonian basins of W Norway.
1176 *Tectonophysics* 608, 1073–1085.
- 1177 Sözbilir, H., 2001. Extensional tectonics and the geometry of related macroscopic structures:
1178 field evidence from the Gediz detachment, western Turkey. *Turk. J. Earth Sci.* 10, 51–67.
- 1179 Spakman, W. and Wortel, R., 2004. A tomographic view on Western Mediterranean
1180 geodynamics. In: W. Cavazza, F.M. Roure, W. Spakman, G.M. Stampfli and P.A. Ziegler
1181 (Editors), *The TRANSMED Atlas - The Mediterranean region from crust to Mantle*.
1182 Springer, Berlin, Heidelberg, pp. 31-52.
- 1183 Taillefer, A., Soliva, R., Guillou-Frottier, L., Le Goff, E., Martin, G., Seranne, M., 2017. Fault-
1184 Related Controls on Upward Hydrothermal Flow: An Integrated Geological Study of the
1185 Têt Fault System, Eastern Pyrénées (France). *Geofluids*, 2017.
- 1186 Tarcan, G., Gemici, Ü., 2003. Water geochemistry of the Seferihisar geothermal area, Izmir,
1187 Turkey. *J. Volcanol. Geotherm. Res.* 126, 225–242.
- 1188 Tarcan, G., Filiz, S., Gemici, U., 2000. Geology and geochemistry of the Salihli geothermal
1189 fields, Turkey. *Books Proc.* 1829–1834.
- 1190 Taylor, H. P., 1974. The application of oxygen and hydrogen isotope studies to problems of
1191 hydrothermal alteration and ore deposition. *Economic geology*, 69(6), 843-883.

- 1192 Tekin, S., Akin, S., 2011. Estimation of the Formation Temperature from the Inlet and Outlet
1193 Mud Temperatures while Drilling Geothermal Formations, in: Proceedings of 36th
1194 Workshop on Geothermal Reservoir Engineering. Stanford University, Stanford.
- 1195 Temiz, U., Eikenberg, J., 2011. U/Th dating of the travertine deposited at transfer zone between
1196 two normal faults and their neotectonic significance: Cambazli fissure ridge travertines (the
1197 Gediz Graben-Turkey). *Geodinamica acta*, 24(2), 95-105.
- 1198 Tezcan, A.K., 1995. Geothermal explorations and heat flow in Turkey. *Terr. Heat Flow*
1199 *Geotherm. Energy Asia* 23–42.
- 1200 Tureyen , O., Gulgor, A., Erkan, B., Satman, A., 2016. Recent expansions of power plants in
1201 Figiris concession in the Germencik geothermal field, Turkey. In Proceedings.
- 1202 Ulugergerli, E. U., Seyitoğlu, G., Başokur, A. T., Kaya, C., Dikmen, U., Candansayar, M. E.,
1203 2007. The geoelectrical structure of northwestern Anatolia, Turkey. *Pure and Applied*
1204 *Geophysics*, 164(5), 999-1026.
- 1205 Vengosh, A., Helvacı, C., Karamanderesi, İ.H., 2002. Geochemical constraints for the origin of
1206 thermal waters from western Turkey. *Appl. Geochem.* 17, 163–183.
- 1207 Wannamaker, P. E., Hasterok, D. P., Doerner, W. M., 2006. Possible magmatic input to the
1208 Dixie Valley geothermal field, and implications for district-scale resource exploration,
1209 inferred from magnetotelluric (MT) resistivity surveying. In *GRC 2006 Annual Meeting:*
1210 *Geothermal Resources-Securing Our Energy Future*.
- 1211 Wortel, M.J.R. and Spakman, W., 2000. Subduction and slab detachment in the Mediterranean-
1212 Carpathian region. *Science*, 290: 1910-1917.
- 1213 Yildirim, N., Aydogdu, O., Sarp, S., 2005. Constraint problems and solution alternatives for
1214 potentially available integrated geothermal energy utilization in Turkey. *Proc. World*
1215 *Geotherm. Congr.* April 24–29.
- 1216 Yılmazer, S., Karamanderesi, İ., 1994. Kurşunlu jeotermal alanının (Salihli-Manisa) jeolojisi ve
1217 jeotermal potansiteli. *Dünya Enerji Konseyi Türkiye* 6, 17–22.
- 1218 Yılmazer, S., Pasvanoğlu, S., Vural, S., 2010. The relation of geothermal resources with young
1219 tectonics in the Gediz graben (West Anatolia, Turkey) and their hydrogeochemical
1220 analyses. In *Proceedings World Geothermal Congress* (pp. 1-10).

1221 **Tables**

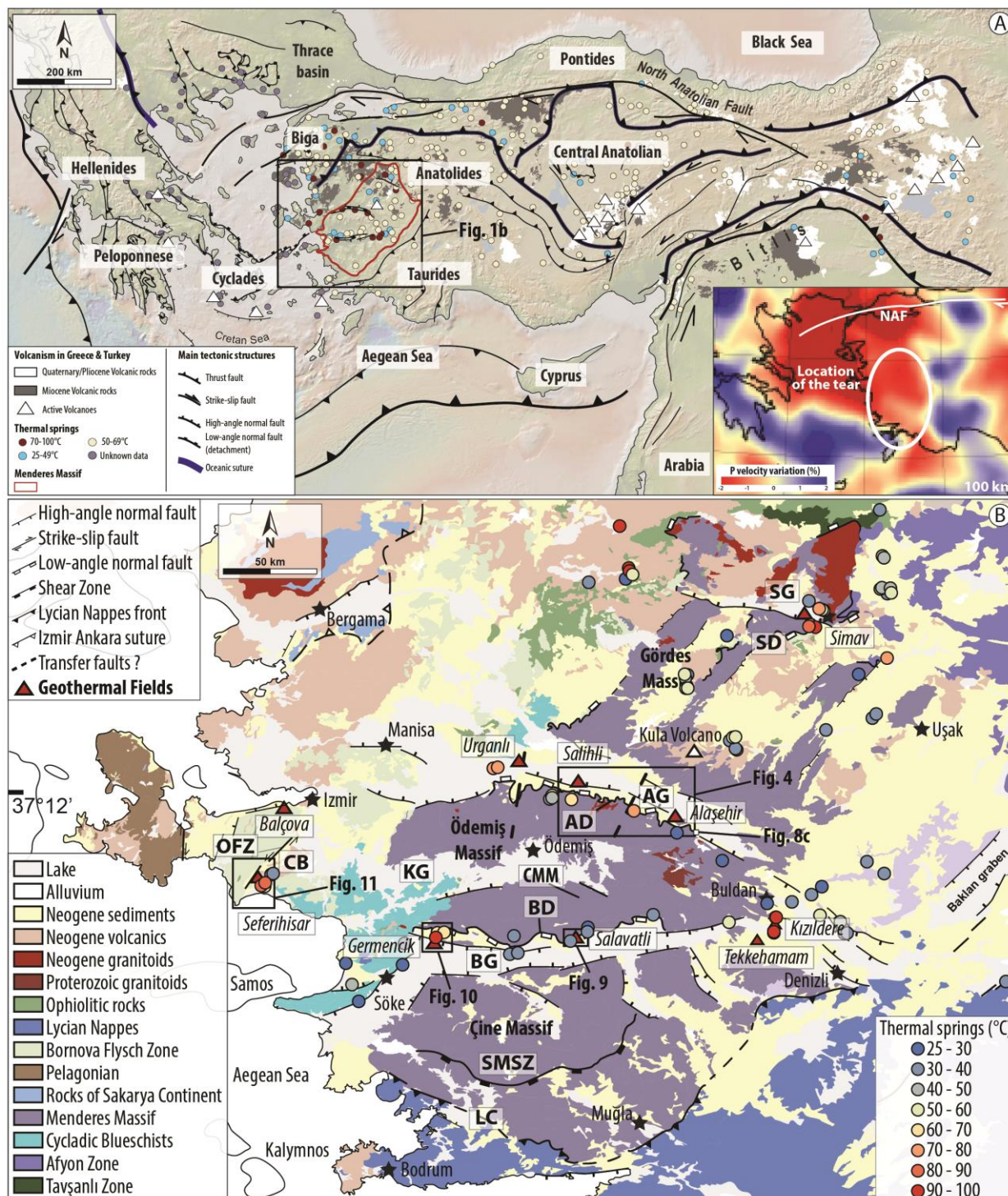
1222 **Table1:** Catalogue of hot springs and geothermal fields associated with the metamorphic core
1223 complex formation in the Menderes Massif. ADFP: Alaşehir detachment fault plane. Compilation
1224 data from Simşek (1984; 2003), Simsek and Demir (1991), Yılmazzer and Karamanderesi (1994),
1225 Karamanderesi (1997; 2013), Özgür *et al.* (1998a; 1998b), Tarcan *et al.* (2000); Gemeci and
1226 Tarcan (2002), Tarcan and Gemeci (2003), Yildirim *et al.* (2005), Kose (2007), Faulds *et al.*
1227 (2010), Kindap *et al.* (2010), Tekin and Akin (2011), Özen *et al.* (2012), Baba *et al.* (2014 ; 2015),
1228 Akin *et al.* (2015) and Tureyen *et al.* (2016).

1229
1230 **Table 2:** Main controls on geothermal fields in the Menderes Massif. BD: Büyük Menderes
1231 detachment, BM: Bornova Mélange, FC: Fault controlled, FRC: Fracture controlled, FW: Foot
1232 wall, AD: Alaşehir detachment, HW: Hanging wall, KC: Karstic controlled, MU: Menderes Unit,
1233 NF: Normal fault.

1234

1235 **Figure Captions:**

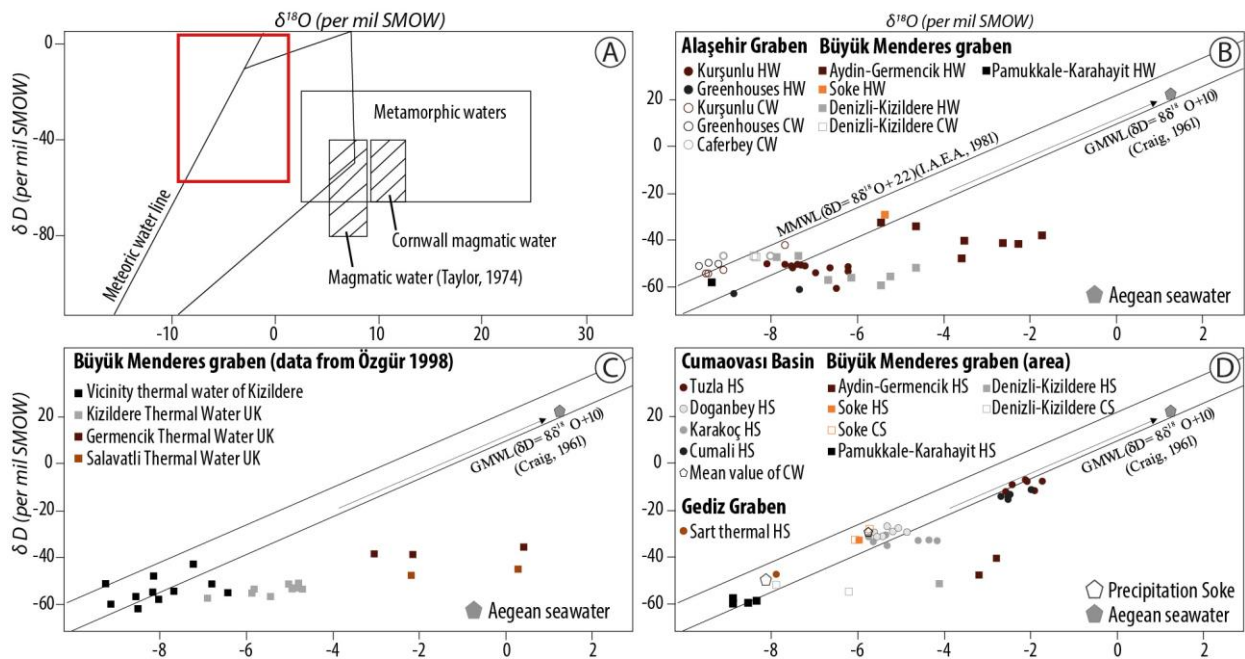
1236



1237
 1238 **Fig. 1:** Tectonic map of Eastern Mediterranean region highlighting the main tectono-metamorphic
 1239 domains and showing location of the study area. Modified from Jolivet *et al.* (2013) and Gessner
 1240 *et al.* (2013). (a) Simplified tectonic map showing major thermal occurrences based on a
 1241 compilation of several data sources (Akkuş *et al.* 2005; Bayram and Simsek 2005, Mendrinos *et*
 1242 *al.* 2010 and Andritsos *et al.* 2015) and spatial distribution of Upper Tertiary-Quaternary

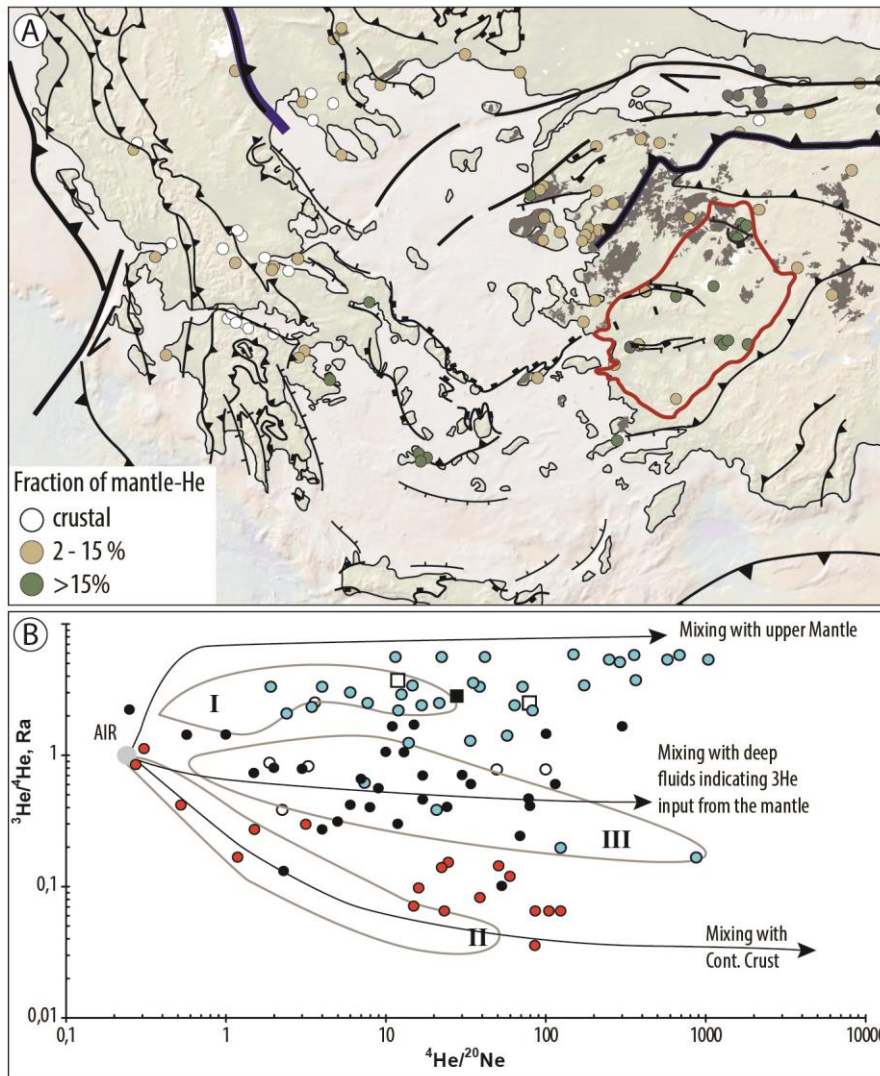
1243 volcanics rocks (from the geological map of the MTA). Note that white triangles indicates active
 1244 volcanoes. Base maps made with *GeoMapApp* (<https://www.geomapp.org>). Tomographic
 1245 model of Piromallo and Morelli (2003) showing the Vp anomalies at the ~ 100 km depth in the
 1246 bottom right corner of this Figure. The white circle illustrates the schematized position of the slab
 1247 tearing. Note that NAF is the abbreviation for North Anatolian Fault. (b) Tectonic and geological
 1248 map of the Menderes Massif modified from the geological map of the MTA and Bozkurt *et al.*
 1249 (2011). Red triangles represent main geothermal areas of the Menderes Massif, from Faulds *et al.*
 1250 (2010) and Kaya (2015). Thermal spring locations correspond to our study, and to the studies
 1251 from Akkuş *et al.* (2005) and Bayram and Simsek (2005). Also indicated is the position of the
 1252 Figs. 4, 8c, 9, 10 and 11. Main structures and grabens are indicated in abbreviations: AD (Alaşehir
 1253 detachment); AG (Alaşehir graben); BD (Büyük Menderes detachment); BG (Büyük Menderes
 1254 graben); CB (Cumaovası basin); CMM (Central Menderes Massif); KG (Küçük Menderes
 1255 graben); LC (Lycian contact); OFZ (Orhanlı fault zone); SMSZ (Southern Menderes shear zone);
 1256 SD (Simav detachment) and SG (Simav graben).

1257



1258

1259 **Fig. 2:** δD vs $\delta^{18}O$ diagrams. (a) Plot of δD vs $\delta^{18}O$ diagram for different water types. The field
1260 of magmatic water and formation waters are taken from Taylor (1974). The field for magmatic
1261 waters from the granites of Cornwall is from Sheppard (1977). The meteoric water line is from
1262 Epstein *et al.* (1965). The metamorphic water field combines the values of Taylor (1974) and
1263 Sheppard (1981). Red rectangle indicates the field of all isotopic data from the Menderes Massif.
1264 (b) Stable isotope compositions of the geothermal reservoir fluids in the studied areas showing
1265 hot and cold waters wells. Abbreviations: HW (Hot water well), CW (Cold water well). (c) Stable
1266 isotopes of different geothermal fields in the Büyük Menderes Graben. Abbreviation: UK
1267 (unknown sampling locations). (d) Stable isotopes of springs in three main basins. Abbreviations:
1268 HS (Hot spring), CS (Cold spring). Compilation of data from Filiz *et al.* (2000), Özgür (2002),
1269 Tarcan and Gemici (2003), Simsek (2003) and Özen *et al.* (2012).
1270



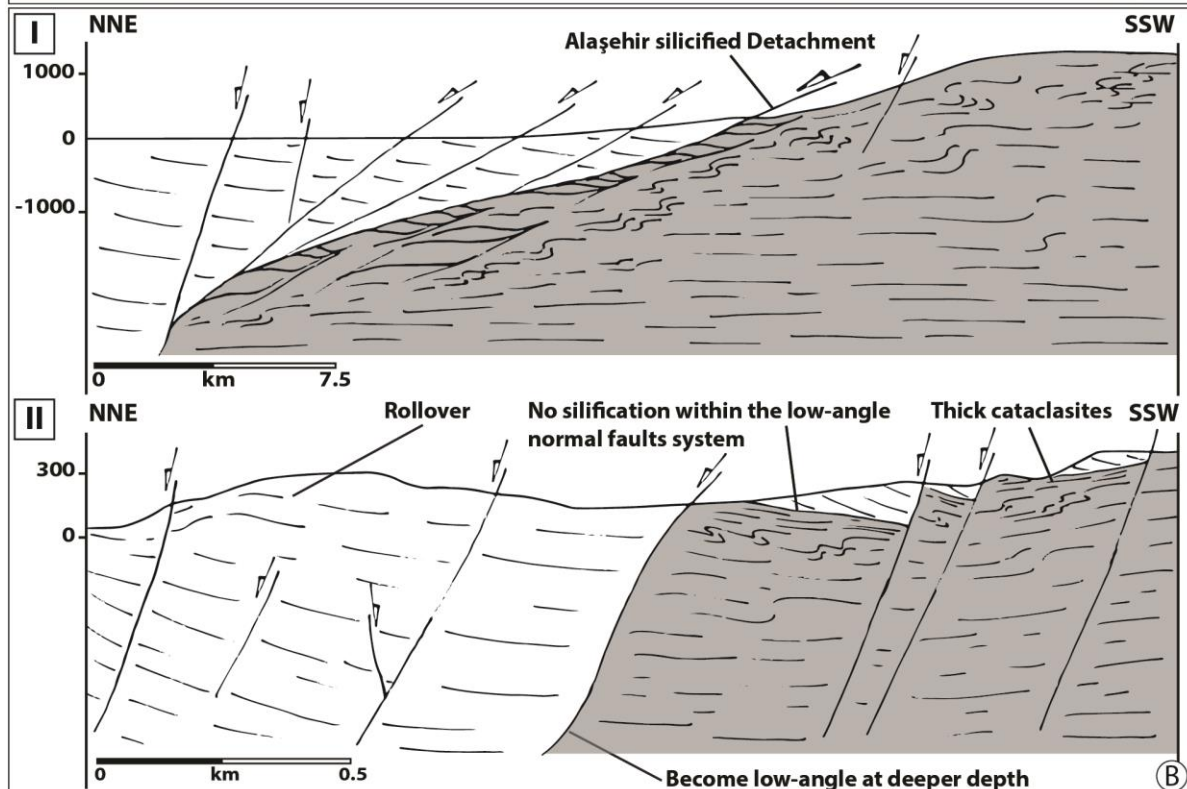
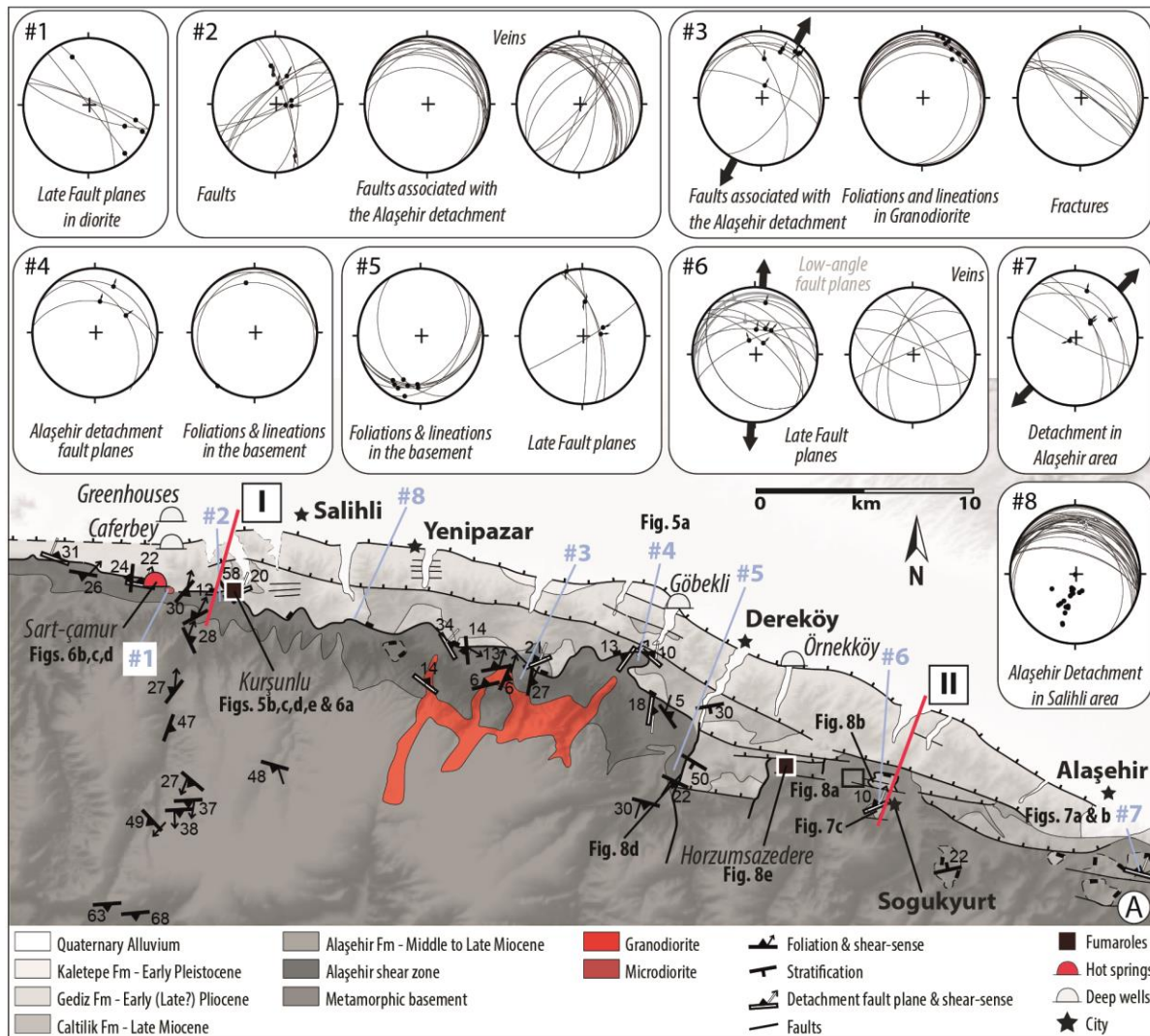
1271

1272 **Fig. 3:** Isotopic composition of Helium. (a) Fraction of mantle-He in hydrothermal fluids from
 1273 the Aegean Anatolian domains computed from helium isotopic data, assuming mixing between a
 1274 crustal component (0.04 Ra) and a mantle component (8 Ra), modified from Pik and Marty (2009).
 1275 Helium isotopic data are from Pik and Marty (2009) and Karakuş (2015). (b) R/Ra diagram for
 1276 the Eastern Mediterranean region from Güleç (1988), Güleç *et al.* (2002), Güleç and Hilton
 1277 (2006), Mutlu *et al.* (2008), Pik and Marty (2009) and Karakuş (2015). Black dots showing data
 1278 of the west Anatolian domain, red dots data of the gulf of Corinth, Blue dots data of the magmatic
 1279 arc and white dots data of the back arc region in Greece. In addition, white and black squares
 1280 indicate respectively the Denizli and Kula areas which are located in the Menderes Massif. The
 1281 fields of the three groups of hydrothermal fluids (Pik and Marty 2009), are also presented: I = arc

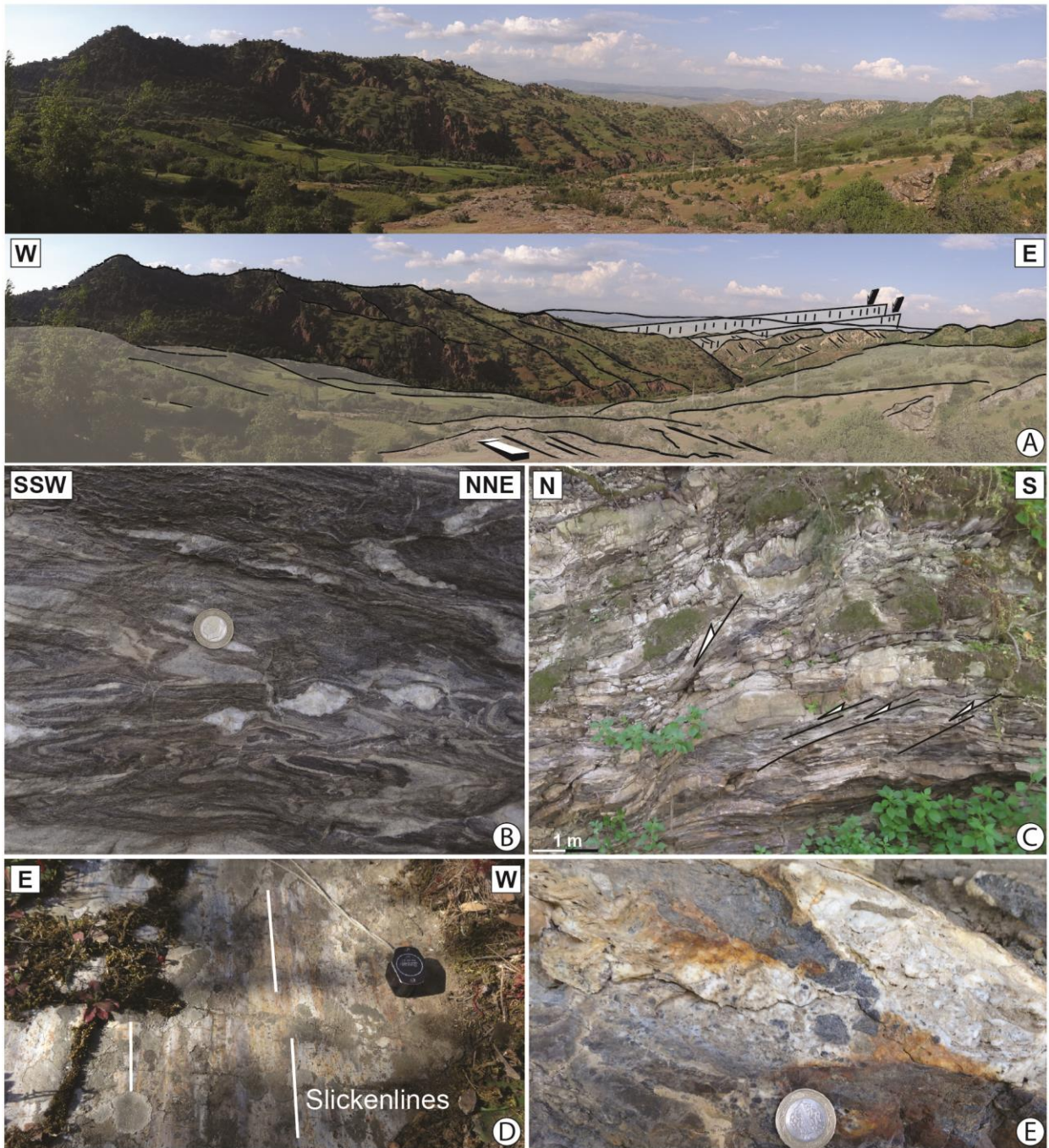
1282 magmatic fluids (>15% mantle-He), II = crustal signature (<1% mantle-He), III = other

1283 intermediate fluids (2–15% mantle-He).

1284



1286 **Fig. 4:** Geological and tectonic map of the Alaşehir graben modified from Asti (2016). (a) Map
1287 showing main structures: the Alaşehir low-angle normal fault, E-W striking high-angle normal
1288 faults and N-S striking high strike-slip faults which are described by Çiftçi and Bozkurt (2010).
1289 Thermal springs and fumarole activity are also located in the map. Brittle structures, foliation,
1290 veins and fractures are presented in Schmidt's lower hemisphere equal-area projection. Detailed
1291 results of the fault slip data inversion are also presented using the Win-Tensor software (Delvaux
1292 & Sperner, 2003). Also indicated is the position of the Figs. 5, 6, 7 and 8. (b) Cross-sections
1293 through the northern part of the Ödemiş Massif. Sections are all roughly parallel to the tectonic
1294 transport. To draw the shape of stratification, we used the bedding data of the Neogene sediments
1295 from Asti (2016). Colours show different rock types. Cross-sections are indicated by red solid
1296 lines in Fig. 4a.
1297



1298

1299

1300

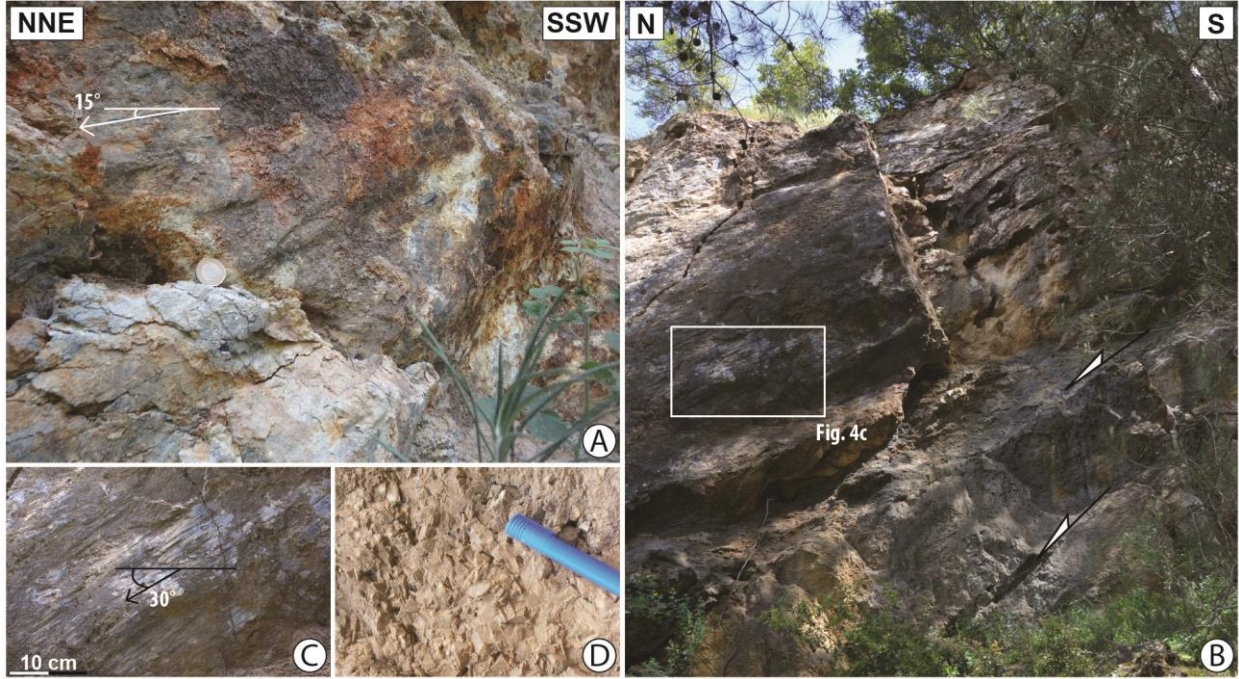
1301

1302

1303

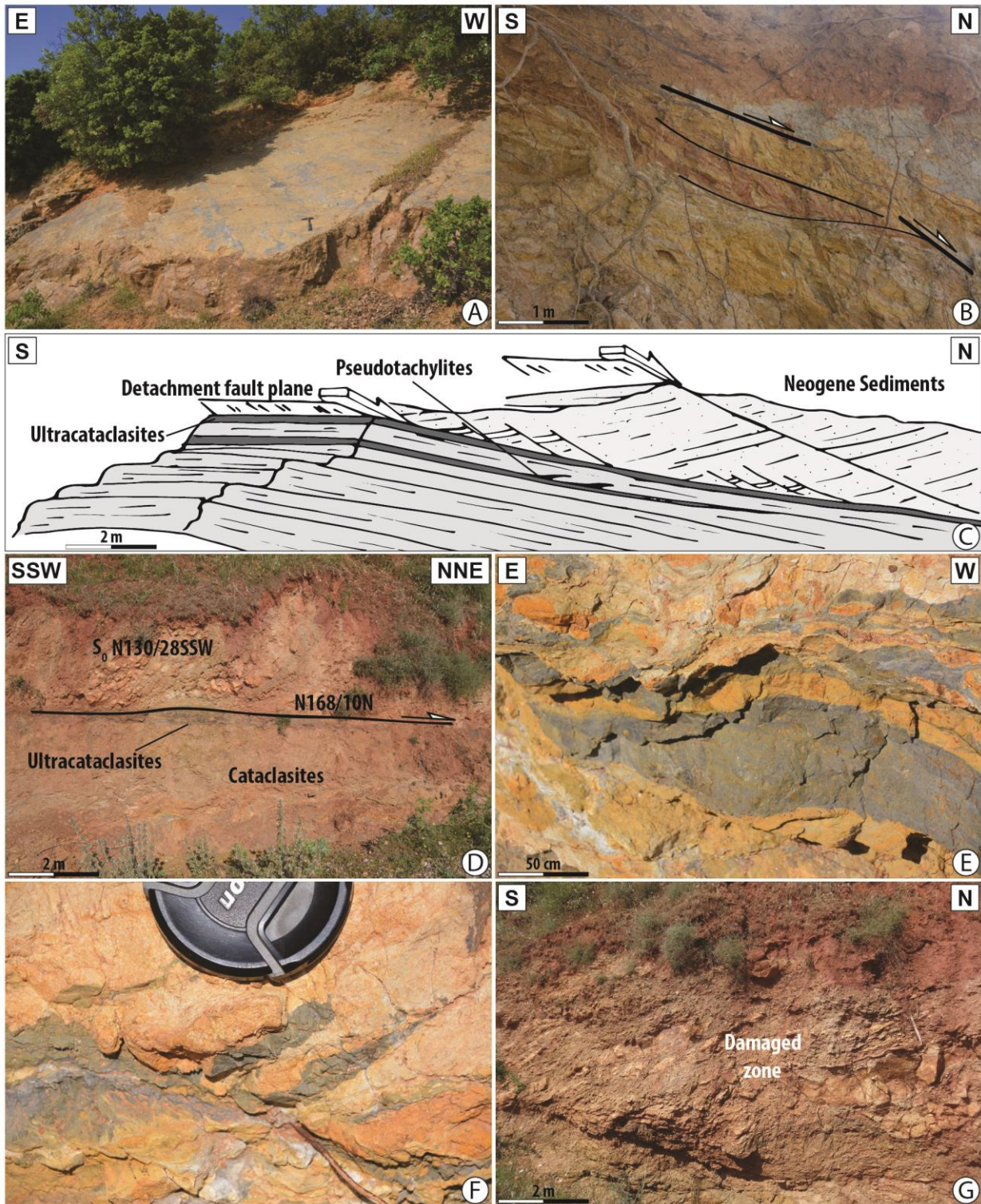
Fig. 5: Kinematic of deformation associated with the Alaşehir detachment. (a) Large-scale view of the Alaşehir detachment surface close to Salihli area. (b) Asymmetric boudins compatible with top-to-the-NNE ductile deformation in marbles layers. (c) Representative outcrop recognized as demonstrative of a brittle stage subsequently developed after the ductile one where shear zones are locally reactivated in the brittle field. (d) Fault plane of the Alaşehir detachment with

1304 slickenlines. (e) Calcite and quartz vein parallel to the bedding, located few meters below the main
1305 fault plane. The position of the pictures is indicated in Fig. 4a.
1306



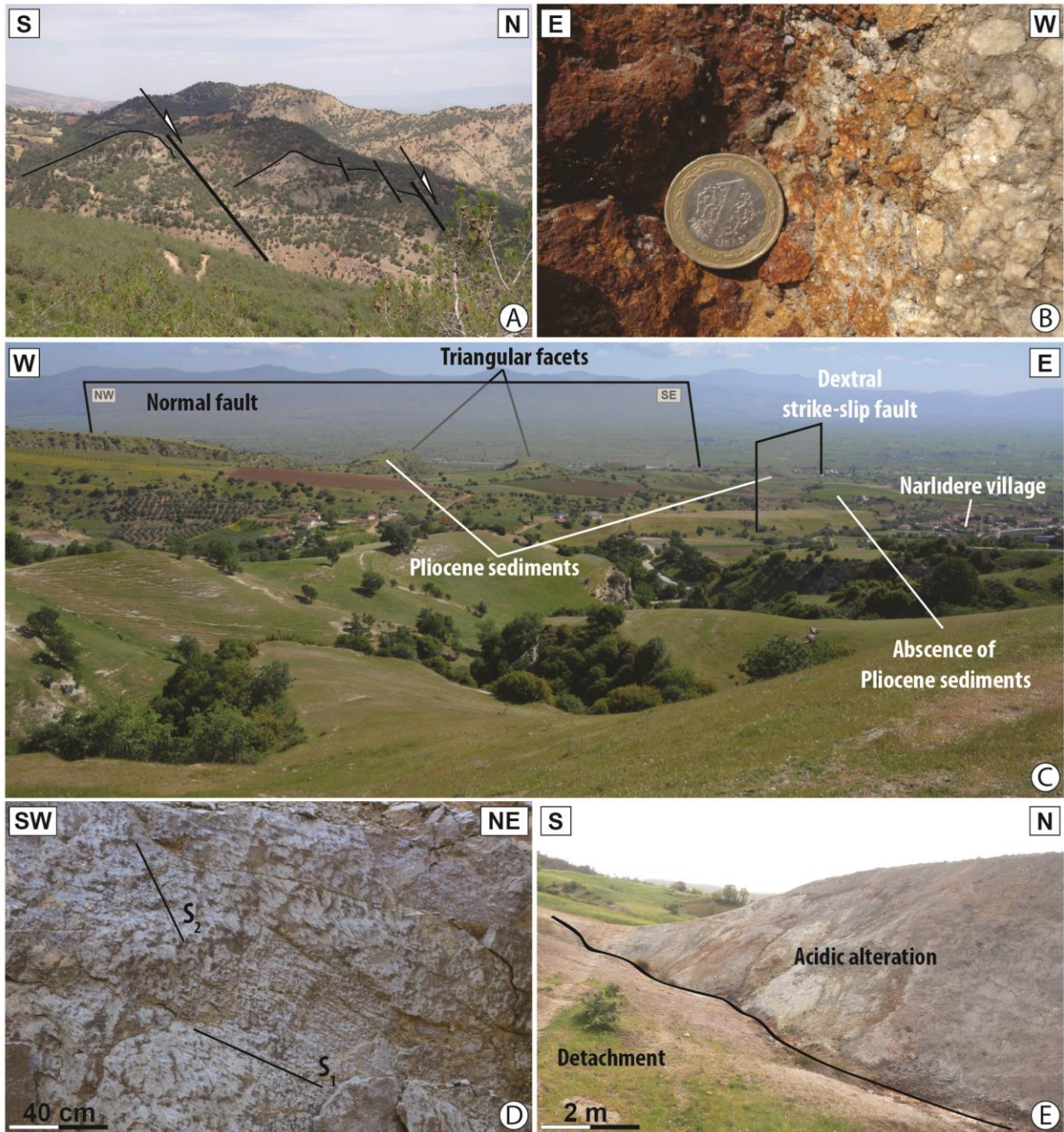
1307
1308 **Fig. 6:** Brittle deformation in the Salihli area. (a) N-S strike-slip fault in the Kurşunlu valley. (b)
1309 E-W striking normal faults are cross-cut by N-S strike-slip fault. (c) Close-up view of a slip-plane
1310 in the basement of the Menderes indicating nearly horizontal with a normal component
1311 slickenlines. (d) Calcite indicating fluid circulation close to the strike-slip fault. The position of
1312 the pictures is indicated in Fig. 4a.

1313



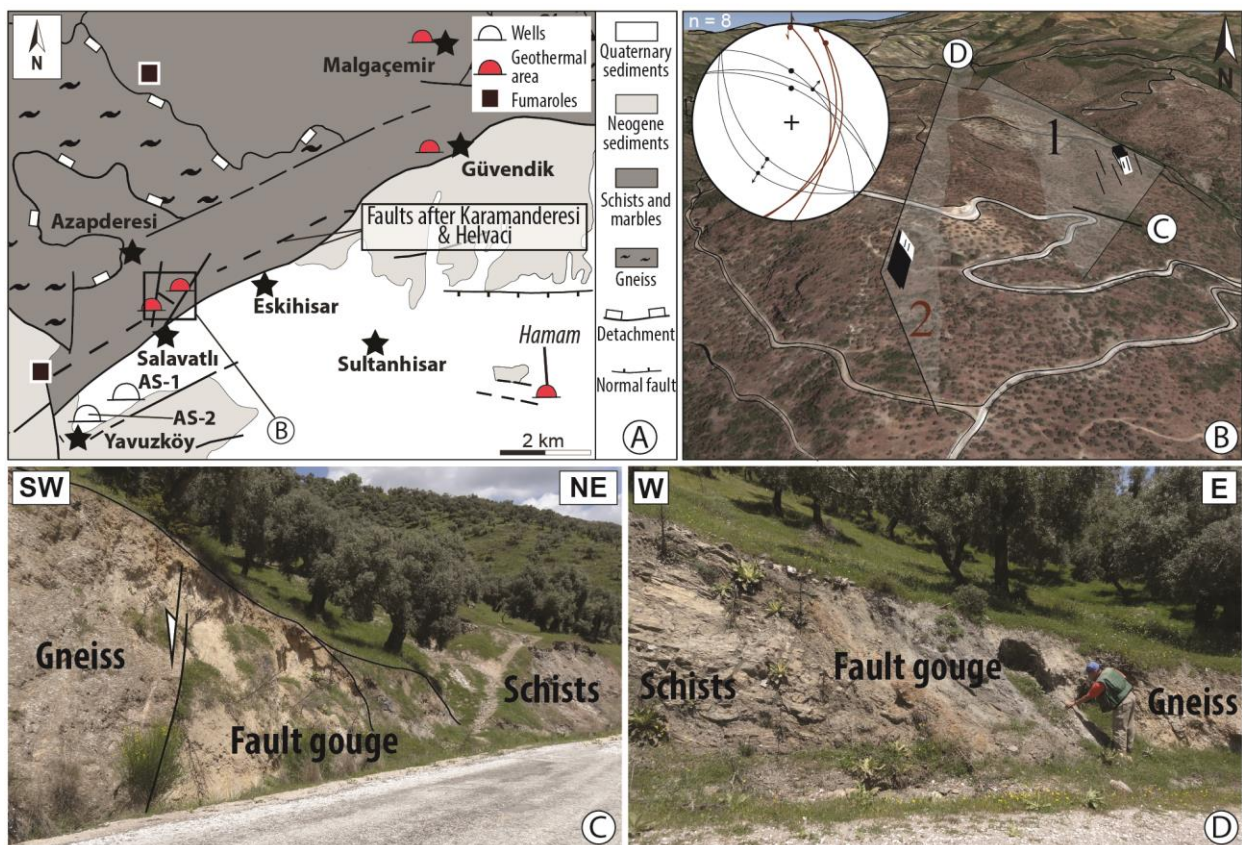
1314
 1315 **Fig. 7:** Brittle deformation associated with the Alaşehir detachment in the Alaşehir area. (a)
 1316 Detachment surface marked by a thick zone of cataclasites. (b) Foliated cataclasites below the
 1317 main fault plane. Note that the shearing is toward the north. (c) Sketch depicting the relationships
 1318 between the detachment fault plane and Neogene sediments in the NNW of Kara Kirse. (d) Low-

1319 angle contact between metamorphic rocks (augen gneiss unit) and Neogene sediments. (e) and (f)
 1320 Close-up view of ultracataclasites and centimetric pseudotachylytes, respectively. (g) Metric
 1321 damaged zone in sediments. The position of the pictures is indicated in Fig. 4a.
 1322

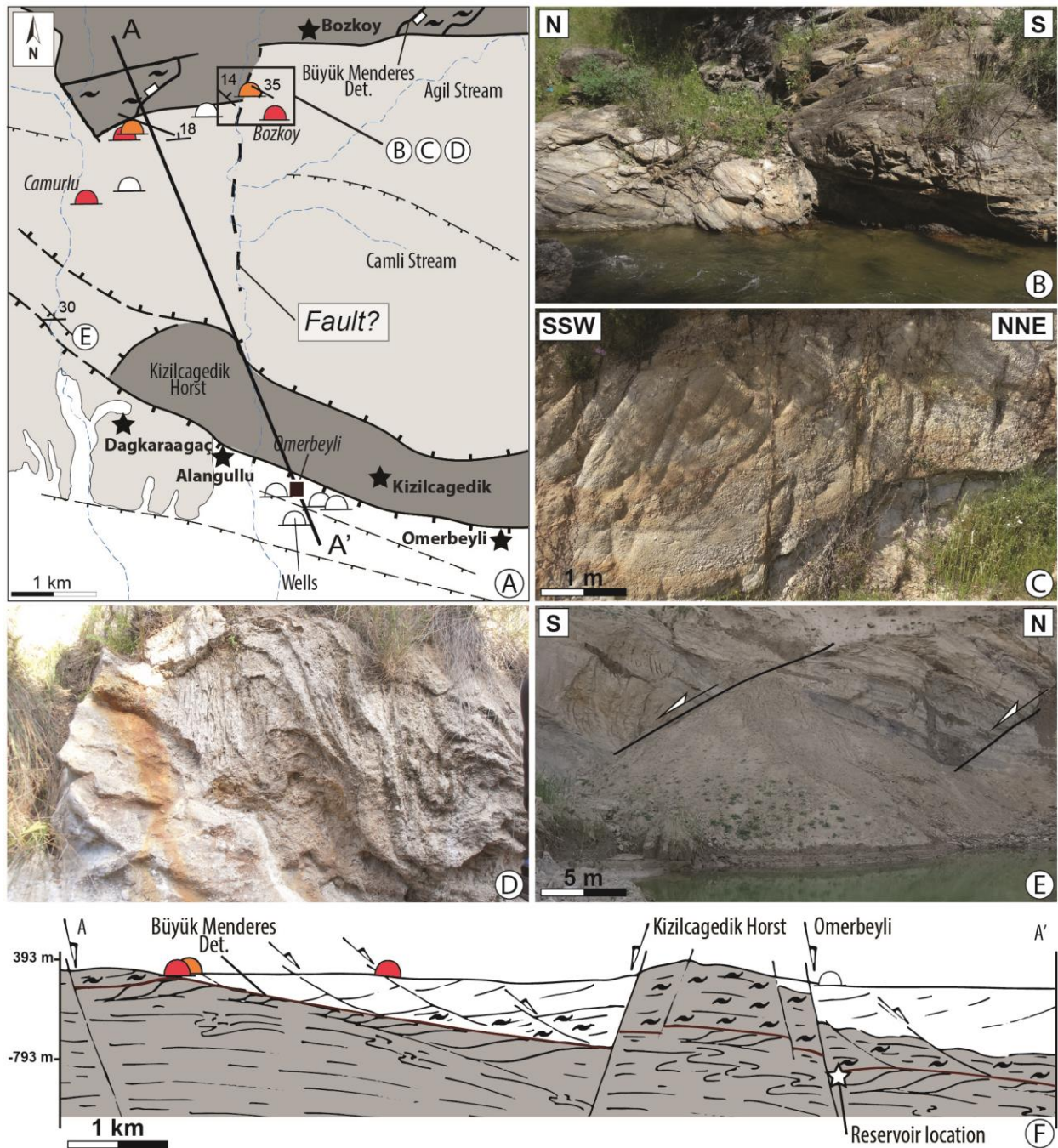


1323
 1324 **Fig. 8:** Brittle deformation in the Alaşehir area. (a) Large-scale E-W high-angle normal faults.
 1325 Outcrop shows hanging wall displacements toward the north. (b) Close-up view of E-W striking
 1326 fault showing centimetric and angular blocs (*i.e.* cataclase). Note also the alteration of the

1327 basement rocks implying a probable meteoric fluid circulation during fault activity. (c) Land-
 1328 scape view of triangular facets in the eastern part of Alaşehir. Note the probable position of strike-
 1329 slip fault. This fault is also mapped by Oner and Dilek (2013). See location in Fig. 4a. (d) Fault
 1330 plane and associated striae (two generations) of N-S striking strike-slip fault. Note that
 1331 stereographic projection of striated fault planes corresponds to the number #5 in Fig. 4a. (e)
 1332 Picture showing an acidic alteration related to fumarole activity. See Fig. 4a for the location of
 1333 pictures.
 1334



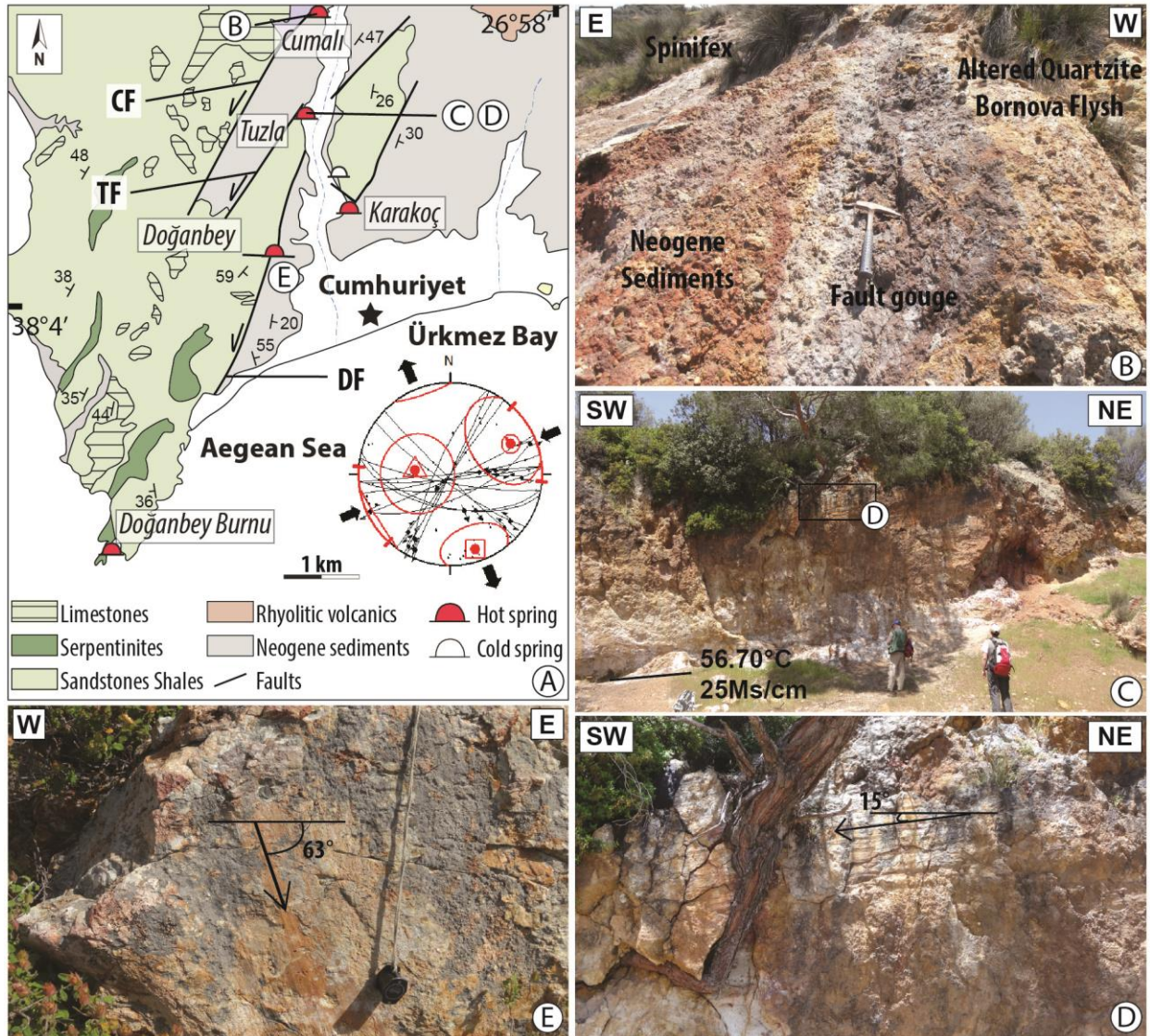
1335
 1336 **Fig. 9:** Brittle deformation in the Salavatlı area. (a) Simplified geological map of Salavatlı
 1337 geothermal field modified from (Karamanderesi and Helvaci, 2003). (b) Google earth view of the
 1338 area. Main structures and stereographic projections of faults systems are indicated. Location is
 1339 indicated in Fig. 9a. (c) NW-SE trending normal fault between gneiss and schists. (d) N-S trending
 1340 faulted contact between schists/marbles sequences and gneiss. Note the metric fault breccia
 1341 between these both units.



1343

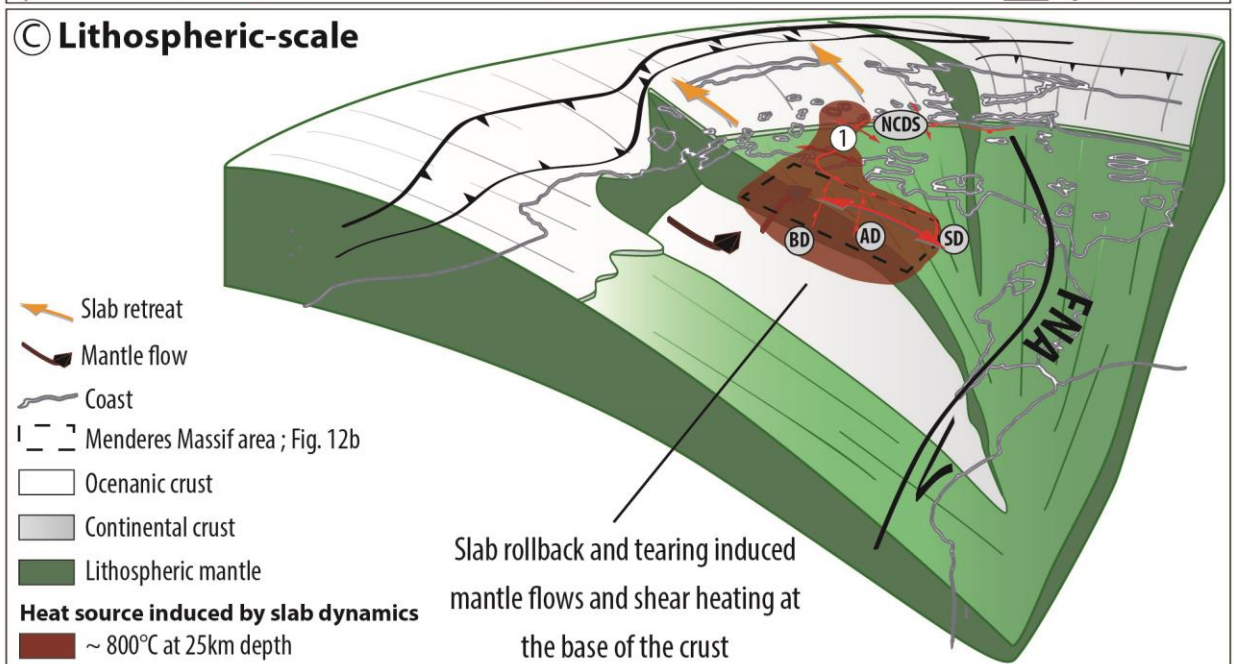
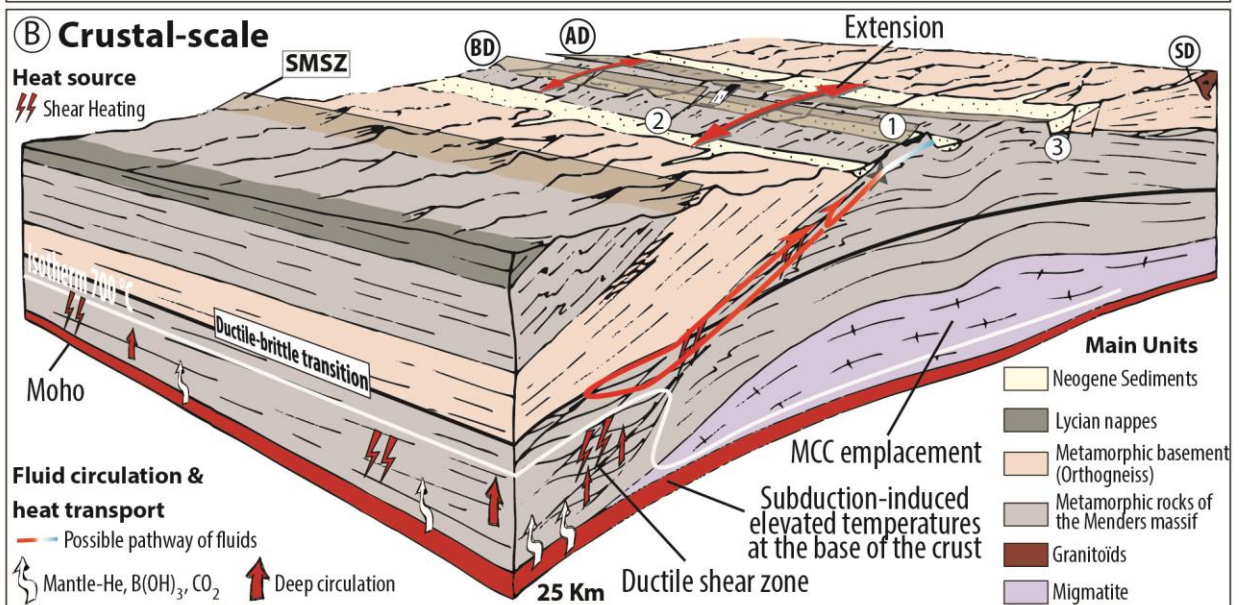
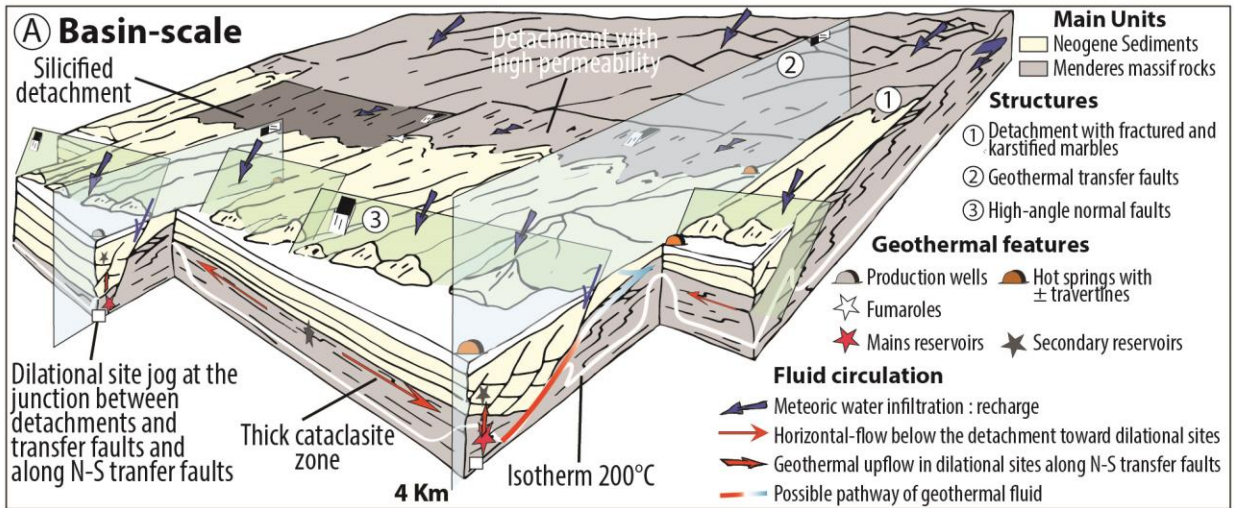
1344 **Fig. 10:** Structures and geothermal activities in the Germencik geothermal field. (a) Simplified
 1345 geological map of Germencik area modified from Karamanderesi (2013), showing thermal
 1346 springs and fumaroles locations. (b) Shallow dipping E-W trending foliation in the basement of
 1347 the Menderes units. (c) Dip inversion of the bedding in Neogene sediments close to the basement.
 1348 (d) Travertine indicating fluid circulation. (e) Sallow dipping E-W striking fault in Neogene

1349 sediments of the Büyük Menderes graben. (f) Simplified cross-section of the Germencik area (see
 1350 location on Fig. 10a).
 1351



1352
 1353 **Fig. 11:** Brittle deformation in the Seferihisar area. (a) Simplified tectonic and geological map of
 1354 Seferihisar geothermal areas showing main structures: the Cumalı Fault (CF), the Tuzla Fault (TF)
 1355 and the Doğanbey Fault (DF). Modified from Genç *et al.* (2001) and Drahor and Berge (2006).
 1356 Also are represented stereographic projections of striations and kinematics of the main fault
 1357 planes. (b) CF showing the altered contact between the basement and Neogene sediments. (c)
 1358 Field photograph of TF plane in the Bornova mélange showing a NNE-SSW trending. Note the
 1359 strong alteration at the foot of the fault implying the presence of hot spring. (d) Close-up view of

1360 the fault plane showing well-preserved slickenlines. (e) Fault plane and associated striae
1361 belonging to the E-W trending normal fault. See Fig. 11a for location.
1362



1364 **Fig. 12:** Conceptual models at different scales showing the heat source origin and main structural
1365 controls on fluid flows in the Menderes Massif. (a) Synthetic simplified block diagram at basin-
1366 scale showing the relationships between these faults. Numbers show different type of faults.
1367 Geothermal features and fluid circulation are also indicated. (b) Role of the detachment on deep
1368 circulation in the Menderes Massif. Main structures are indicated in abbreviations: AD (Alaşehir
1369 detachment); BD (Büyük Menderes detachment); SD (Simav detachment) and SMSZ (Southern
1370 Menderes shear zone). (c) Tentative 3D reconstruction and flow directions in the mantle (red
1371 arrows) of the Aegean region before the recent slab tear below the Corinth Rift and after. Red
1372 line and red arrows show the main detachments and kinematic of extension in this region,
1373 respectively. Yellow arrows indicate the slab retreat in the Aegean domain. Main structures are
1374 indicated in abbreviations: AD (Alaşehir detachment), BD (Büyük Menderes detachment), NAF
1375 (North Anatolian Fault), NCDS (North Cycladic Detachment System) and SD (Simav
1376 detachment).

	<i>Geothermal fields</i>	<i>Depth & Thickness</i>	<i>Flow & Discharge rates</i>	<i>Measured temperatures</i>	<i>Chemical geothermometers</i>	<i>Lithology</i>	<i>Capfault and caprock</i>	
Alaşehir graben	<i>Salihli</i>	Reservoir depth varies from 40–400 m	20 L/s (K-1) and 40 to 80 L/s (other wells in Kurşunlu area)	83–94°C		Karstified and fractured marbles of the basement; Çaltılık Formation	Siliceous ADFP and Gediz Formation	
		Reservoir depth from 950–1500 m	30 to 35 L/s	90–92°C				
	<i>Alaşehir</i>	Reservoir depth from 1150 m and 1600 m	12 L/s (KG-1) and 6,74 L/s (Ak-2)	215°C (A5-2)				80° to 250°C (with variability of geothermometers e.g., SiO ₂ ; Quartz Steam Loss; Na-K-C)
		Reservoir depth from 1750 to 2750 m	5–90 L/s	159–287,5°C				
<i>Urganlı-Turgutlu</i>	Reservoir depth at 460 m	20 L/s	62°C	-	-			
Büyük Menderes graben	<i>Germencik</i>	Shallow reservoir depth in sediments (around 285 m)	Average flow rate rate 300 tph	203–217°C	150–250°C (Na-K & Na-K-Ca)	Miocene conglomerates and Fractured rocks of the basement	Neogene clastic sediment such as clayey levels	
		Deeper reservoir in basement changes depending on the locality from 965 to 2432 m depth		191–276°C				
<i>Salavatlı</i>	Reservoir depth from 750–1923 m	Average flow rate 1480 tph	148–176°C	160–175°C (Giggenbach, 1986)	Fissures and fractures zones of the basement	-		

Cumaovası basin		Reservoir depth at 3224 m	-	211°C	-	-
	<i>Kızıldere</i>	First reservoir depth at 400 m		148–198°C		Sazak Formation (Pliocene sediments) and quaztites, marbles, gneiss of the basement
		Second reservoir depth from 1100 m to 1200 m	Average flow rate 1400–1500 tph		200–212°C	
Just below the second				242°C	250–260°C (SiO ₂ ; Na-K-Ca)	
		Fourth reservoir depth unknow	-	>250°C	-	-
	<i>Seferihisar (Tuzla)</i>	Reservoir depth from 333–553 m	Total discharge rates of 130 tph	174–176°C	-	Fractured mafic submarine volcanics and fractured rocks of Bornova mélangé; Marbles of Menderes?
						Clay-rich zones of the Neogene sediments
Simav graben	<i>Simav</i>	First reservoir shallow depth, 85 m		105°C		Neogene sediments: Naşa basalt, Budağan limestone, Arıkaya and Balıkbası formations; Menders units?
		Second reservoir: around 725 m	-	162°C	83 to 182°C (SiO ₂) and 148 to 163°C (Na-K-Ca-Mg)	Clayey level of Eynal, Akdağ and Sarıcasu Formations

	Geothermal fields	Structural setting	Structural characteristics	Main controls
Alaşehir graben	Salihli	HW and FW of the south side of the graben	Intersections between N-dipping detachment, N-S trending strike-slip faults and sometimes E-W trending normal faults	KC, FC, FRC
	Alaşehir	HW and FW of the south side of the graben	Intersections between N-dipping detachment, N-S trending strike-slip faults and sometimes E-W trending normal faults	
	Urganlı-Turgutlu	HW and FW of the north side of the graben	Intersections between N-dipping detachment, N-S trending strike-slip faults in the basin	FC
Büyük Menderes graben	Germencik	HW and FW of the north side of the graben	Intersections between S-dipping detachment, N-S trending strike-slip faults and E-W trending normal faults	FC, FRC
	Salavatlı	HW and FW of the north side of the graben	Intersections between NNE-SSW trending strike-slip faults and SE-NW striking normal faults	
	Kızıldere	HW and FW of the north side of the graben	Eastern termination of major normal fault; Intersections between N-S trending strike-slip faults and E-W striking normal fault	
Cumaovası basin	Seferihisar	HW and FW of the contact between BM/MU	Intersections between N-S transfer faults and the contact between BM/MU	FC
Simav graben	Simav	HW and FW of the north side of the graben	N-dipping detachment and intersections between N-S striking transfer fault and S-dipping normal fault	FC